TURKISH COMPUTATIONAL and THEORETICAL CHEMISTRY

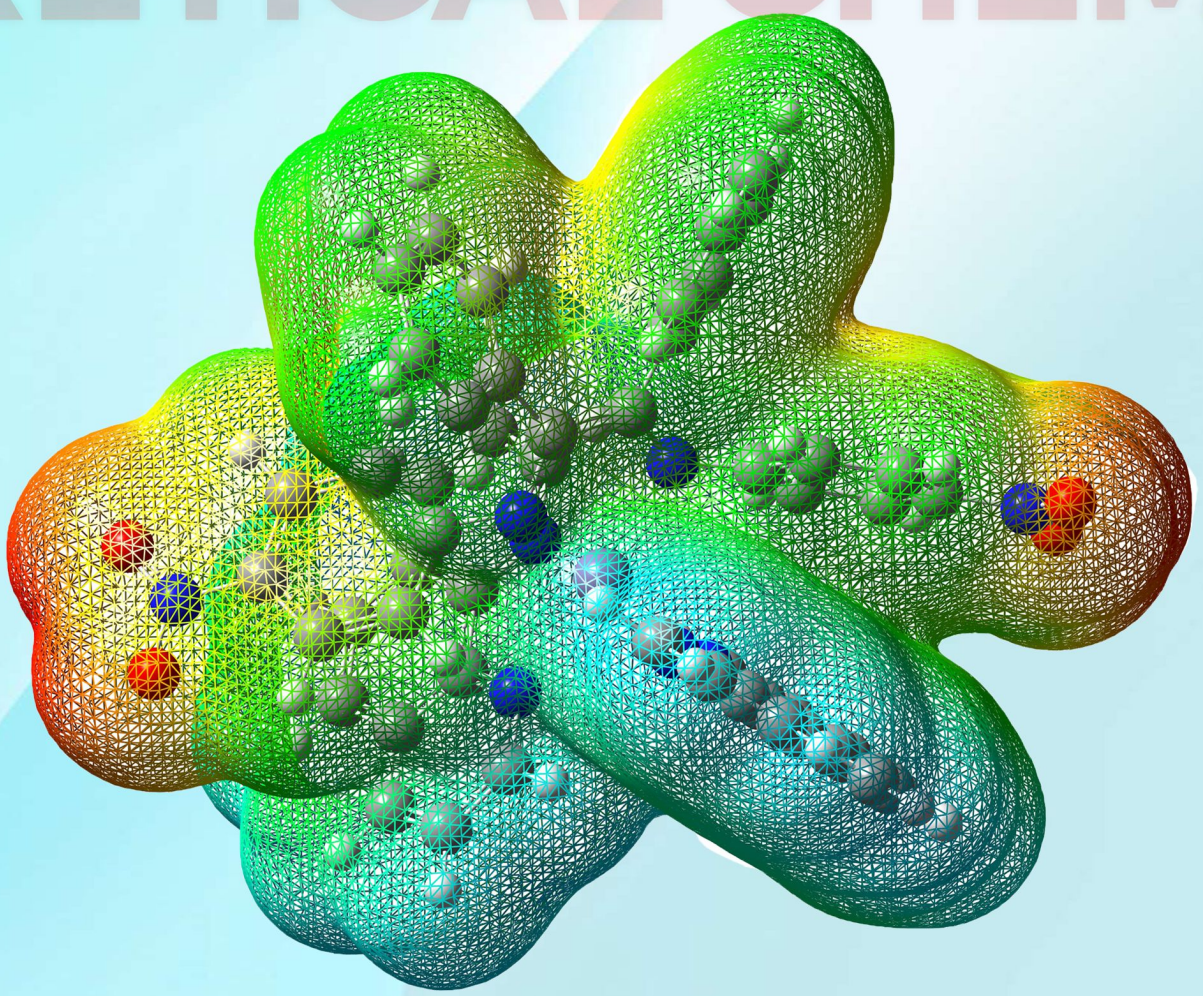

15 DECEMBER 2017 VOLUME: 1 ISSUE: 2

CONTENTS

Turkish Computational and Theoretical Chemistry

Turkish Comp Theo Chem (TC&TC)

Volume(Issue): 1(2) – Year: 2017 – Pages: 1-5

ISSN: 2587-1722 / e-ISSN: 2602-3237

Received: 14.05.2017 ***Accepted:*** 15.06.2017 *Research Article*

Investigation of proton and sodium Ion affinities of topiramate (anticonvulsant drug) by DFT calculations

Hamid Saeidian[1]

Department of Science, Payame Noor University (PNU), PO Box: 19395-4697, Tehran, Iran

Abstract: In this present study, the proton and sodium ion affinities of topiramate has been investigated by density functional theory calculations. The most basic site for protonation on topiramate is nitrogen atom of sulfamate group. It is interesting that sodium ion affinity of topiramate was determined as 670 kJ mol-1 is less than its proton ion affinity. It was found that during sodiation, topiramate conformation is changed. Because of the limited understanding of the biological molecular mechanism of topiramate, these results might devise a clear understanding of the role of topiramate in blockade of voltage-dependent sodium channels in biological systems.

Keywords: *Topiramate, anticonvulsant drug, DFT calculation, sodium ion affinity, Theoretical chemistry, Sulfamate esters.*

Graphical Abstract

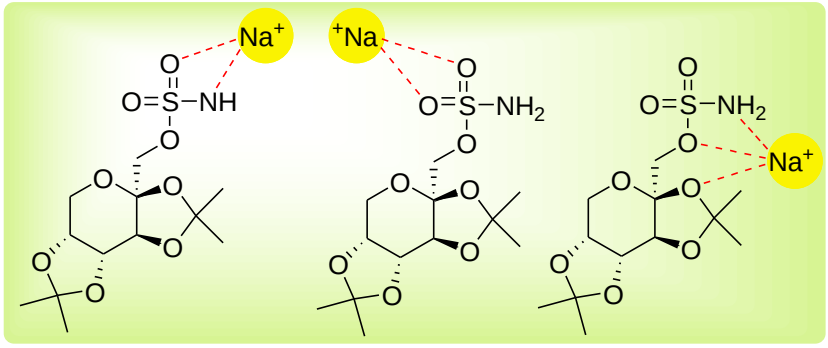

The proton and sodium ion affinities of Topiramate has been investigated by DFT approach. The most basic site for protonation on Topiramate is nitrogen atom of sulfamate group. It is also interesting that sodium ion affinity of Topiramate was determined as 670 kJ mol^{-1} is less than its proton ion affinity. Because of the limited understanding of the biological molecular mechanism of Topiramate, these results might devise a clear understanding of the role of Topiramate in blockade of voltage-dependent sodium channels in biological systems.

[1] Corresponding Author

e-mail: saeidian1980@gmail.com

1. Introduction

Epilepsy has been recognized as a neurological disorder, affecting of people. Every year, approximately 0.25 million new cases are added to this population [1, 2]. Anticonvulsant drugs are useful in treating 90% of the epileptic patients [3]. Compounds bearing sulfamate moiety are an important group of compounds in chemistry and biology. They are widely used in the production of pharmaceuticals and sweeteners [4–6]. Topiramate, namely 2,3:4,5-bis-*O*-(1-methylethylidene)-*β*-D-fructopyranose sulfamate (Figure 1), has emerged as newer and promising anticonvulsant drug marketed worldwide for the treatment of epilepsy [7].

Topiramate is structurally unrelated to other antiepileptic drugs and its biological molecular mechanism of action is still unknown [8-11]. This drug acts by multiple neurostabilizing mechanisms. One of them is blockade of voltage-dependent sodium channels [12, 13].

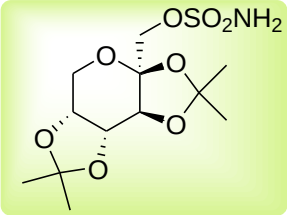

Figure 1. Chemical structure of topiramate.

Topiramate is structurally unrelated to other antiepileptic drugs and its biological molecular mechanism of action is still unknown [8-11]. This drug acts by multiple neurostabilizing mechanisms. One of them is blockade of voltage-dependent sodium channels [12, 13]. Sodium ion, the most important electrolyte, is one of the most abundant metal ions in biological systems. It is involved in a variety of biological processes, including osmotic balance, the stabilization of biomolecular conformations and information transfer *via* ion pumps and ion channels [14-16]. Understanding of topiramate interactions with Na^+ and H^+, and to obtain some information about the intrinsic binding modes of these ions to topiramate, is necessary. The present study addresses this subject by using density functional theory calculations (DFT) calculations.

2. Computational Details

Geometry optimizations and frequency calculations of all species were carried out using the Gaussian 03 program [17]. Density Functional Theory with the Becke three parameters hybrid functional (DFT-B3LYP) calculations were performed with a 6-31G (d) basis set for all atoms. Vibrational frequencies were calculated at the same level to ensure that each stationary point is a real minimum. Harmonic-oscillator approximation was also used for the thermodynamic partition functions. After geometry optimization and frequency calculations, zero-point energies (ZPEs) and thermal corrections are obtained at 298.15 K.

3. Results and discussion

Topiramate structure, was fully optimized in the B3LYP method using 6-31G(d) basis set [18, 19] and then, the most stable conformer is used for proton and sodium ion affinities (see supporting information, Figure 1S). Proton ion affinity for topiramate [PIA (T)] in the gas phase can be defined as the negative value of the enthalpy variation (ΔH) for the process:

$$\text{Topiramate} + H^+ \longrightarrow [\text{TopiramateH}]^+$$

$$\begin{aligned}\mathbf{PIA(T)} &= -\Delta\mathbf{H} = -\Delta\mathbf{E} - \Delta(\mathbf{pv}) = \\ &-\Delta\mathbf{E} - \Delta\mathbf{n}_g\mathbf{RT} = -\Delta\mathbf{E} + \mathbf{RT} = \\ &-\mathbf{E(T{-}H^+)} + \mathbf{E(T)} \\ &+ \mathrm{E(H^+)} + \mathrm{RT} = \\ &-\mathrm{E(T{-}H^+)} + \mathrm{E(T)} + 3/2\mathrm{RT} + \mathrm{RT} = \\ &-\mathrm{E(T{-}H^+)} + \mathrm{E(T)} + 5/2\mathrm{RT}\end{aligned} \quad (1)$$

Like proton ion affinity, sodium ion affinity for topiramate [NaIA (T)] in the gas phase can be assumed:

$$\begin{aligned}\mathrm{NaIA(T)} &= -\Delta\mathrm{H} = -\Delta\mathrm{E} - \Delta(\mathrm{pv}) = \\ &-\mathrm{E(T{-}Na^+)} + \mathrm{E(T)} + \mathrm{E(Na^+)} + \mathrm{RT}\end{aligned} \quad (2)$$

In equations (1) and (2) E is the total energy calculated for the optimized structures of topiramate, protonated and sodiated topiramate at 298.15 K. The 5/2RT term includes the translation energy of proton [20]. Zero point vibrational energies were computed in order to correct all the calculations to 298.15 K.

Three basic sites for protonation were assumed on topiramate structure: the nitrogen atom of amino group (A), the oxygen atom of sugar ring (B, C—O—C) and the oxygen atom of O=S moiety (C). The most stable corresponding protonic structures of protonated topiramate are shown in Figure 2. The isomer A is stabilized by two intramolecular hydrogen bonds between amino group and oxygen atoms of sugar unit. Due to positive charge of nitrogen atom on amino group, these intramolecular hydrogen bonds in A, are more strong than the others. The proton ion affinity (P*IA*) and the proton ion affinity difference (ΔP*IA*) between these species are given in Table 1. The results show that among the three basic sites, the amino group has the greatest P*IA*. The proton ion affinity of the NH_2 group is estimated to be 27 kJ mol^{-1} and 57 kJ mol^{-1} higher than of oxygen atoms of sugar ring and O=S, respectively at the B3LYP/6-31G(d) level.

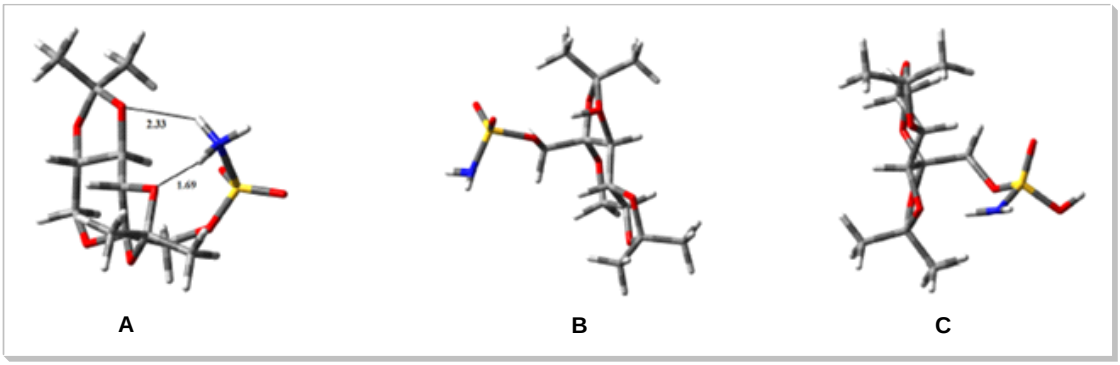

Figure 2. Optimized protonated isomers of topiramate at B3LYP/6-31G(d) level (distances are in Å).

Table 1. *PIA* and ΔP*IA* of optimized protonated isomers of topiramate determined in kJ mol^{-1}.

P*IA*(**A**)	P*IA*(**B**)	P*IA*(**C**)	ΔP*IA*(**A-B**))	ΔP*IA*(**A-C**)
919	892	862	27	57

In the next step, calculations were performed for topiramate complexes corresponding to the position known as the active sites for the interaction of sodium ion. As seen in Scheme 1, in principle, sodium ion can interact with topiramate at different positions: (1) on a nitrogen of amine, oxygen atom of O=S, oxygen atoms of sugar ring; (2) on combination of 1, 2 and 3 situations as a tri-coordinated or bi-coordinated ligand (see supporting information, Figure 3S). The optimized structures of some sodiated conformers of topiramate are given in Figure 4S of supporting information.

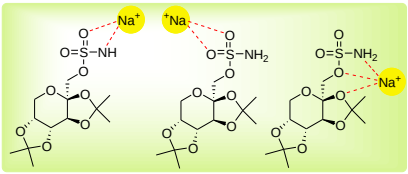

Scheme 1. Some of the initial structures used for complexation of topiramate with sodium ion.

The results of calculations show that during metalation, the topiramate conformation is changed significantly. As can be seen from Figure 3, the tri-coordinated complex, is the most stable sodiated conformer of topiramate, in which the sodium has attractive electrostatic interactions with the oxygen atoms of sugar ring and O=S group. Sodium ion affinity for topiramate [Na*IA* (T)] in the gas phase using the equation (2) for the most stable conformer was calculated to be 249 kJ mol^{-1} at the B3LYP/6-31G(d).

4. Conclusion

The amino group has been confirmed to be the most favorable protonation site of topiramate in the gas phase. On the other hand, comparing the calculated ΔH of the reactions:

$$\text{Topiramate} + H^+ \longrightarrow [\text{TopiramateH}]^+ \quad \Delta H = -919 \text{ kJ mol}^{-1}$$

$$\text{Topiramate} + Na^+ \longrightarrow [\text{TopiramateNa}]^+ \quad \Delta H = -249 \text{ kJ mol}^{-1}$$

Indicating that the protonation of topiramate is more exothermic than the sodinization (670 kJ mol^{-1}).

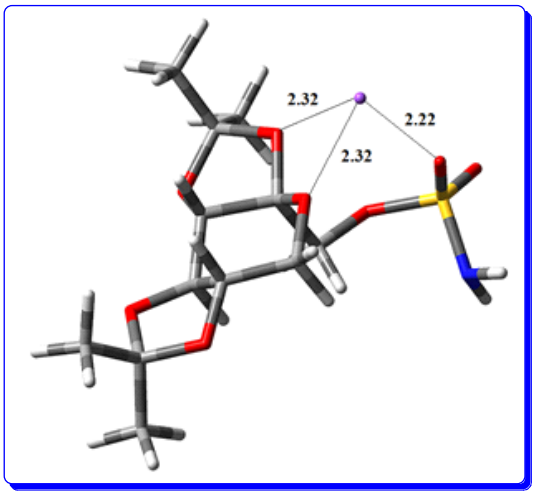

Figure 3. Optimized structure and main geometrical parameters of the most stable conformer of sodiated topiramate at the B3LYP/6-31G(d) level (distances are in Å).

Difference in energies between H^+ and Na^+ reflect the fact that the sodium ion has electrons and hence its positive charge is spread over space while H^+ is a point charge and the positive charge is not spread out at all. These two, therefore, bind with very different energies. DFT calculation results, for the gas phase, can be used as a guideline for the condensed phase and it might devise a clear understanding of the role of topiramate in blockade of voltage-dependent sodium channels in biological systems.

References

[1] E. Spina , G. Perugi, Antiepileptic drugs: indications other than epilepsy, Epileptic Disorders 6 (2004) 57-75.

[2] M.R. Trimble, New Anticonvulsants Advances in the Treatment of Epilepsy, Wiley, New York, 1994, 1-33.

[3] M.J. Brodie, Established anticonvulsants and treatment of refractory epilepsy, The Lancet 336 (1990) 350-354.

[4] H. Saeidian, M. Abdoli, Z. Mirjafary, Synthesis of acyclic and cyclic sulfamates: a Review, Synthesis 47 (2015) 1057-1075.

[5] M. Abdoli, H. Saeidian, Synthesis and reactivity of imidazole-1-sulfonate esters (imidazylates) in substitution, elimination, and metal-catalyzed cross-coupling reactions: a review, Journal of Sulfur Chemistry 36 (2015) 556-582.

[6] H. Saeidian, M. Abdoli, The first general protocol for N-monoalkylation of sulfamate esters: benign synthesis of N-alkyl Topiramate (anticonvulsant drug) derivatives, Journal of Sulfur Chemistry 36 (2015) 463-470.

[7] R.P. Shank, J.F. Gardocki, A.J. Streeter, B.E. Maryanoff, An overview of the preclinical aspects of topiramate: pharmacology, pharmacokinetics, and mechanism of action, Epilepsia 41 (2000) S3-9.

[8] J.W. Winum, A. Scozzafava, J.L. Montero, C.T. Supuran, Sulfamates and their therapeutic potential, Medical Research Review 25 (2005) 186-228.

[9] R.P. Shank, J.F. Gardocki, J.L.Vaught, C.B. Davis, J.L. Schupsky, R.B. Raffa, S.J. Dodgson, S.O. Nortey, B.E.Maryanoff, Topiramate: preclinical evaluation of structurally novel anticonvulsant, Epilepsia 35 (1994) 450-460.

[10] W.E. Rosenfeld, Topiramate: a review of preclinical, pharmacokinetic, and clinical data, Clinical Therapeutics 19 (1997) 1294-1308.

[11] D.F. Zullino, S. Krenz, J. Besson, AMPA blockade may be the mechanism underlying the efficacy of topiramate in PTSD, Journal of Clinical Psychology, 64 (2003) 219-220.

[12] P. Kwan, G.J. Sills, M.J. Brodie, The mechanisms of action of commonly used antiepileptic drugs, Pharmacology Therapeutics 90 (2001) 21-34.

[13] S. Taverna, G. Sancini, M. Mantegazza, S. Franceschetti, G. Avanzini, Inhibition of Transient and Persistent Na+ Current Fractions by the New Anticonvulsant Topiramate, The Journal of Pharmacology and Experimental Therapeutics 288 (1999) 960-968.

[14] J.A. Cowan, Inorganic Biochemistry: An Introduction, 2th ed., Wiley-VCH, New York, 1997.

[15] W. Kaim, B. Schwederski, Bioinorganic

Chemistry: Inorganic Elements in the Chemistry of Life: An Introduction and Guide, Wiley, New York, 1994.

[16] A.R. Michell, The clinical biology of sodium: the physiology and pathophysiology of sodium in mammals, Oxford, UK, 1995.

[17] M.J. Frisch, et al. Gaussian, Inc., Wallingford CT, Gaussian 03, Revision E.01, Gaussian, Inc., Pittsburgh PA, 2003.

[18] M. Ghiasi, A.A. Oskouie, H. Saeidian, Dynamic stereochemistry of Topiramate (anticonvulsant drug) in solution: theoretical approaches and experimental validation, Carbohydrate Research 348 (2012) 47-54.

[19] M. Ghiasi, S. Kamalinahad, M. Arabieh, M. Zahedi, Carbonic anhydrase inhibitors: a quantum mechanical study of interaction between some antiepileptic drugs with active center of carbonic anhydrase enzyme, Carbohydrate Research 992 (2012) 59-69.

[20] M. Shakourian-Fard, A. Fattahi, Z. Jamshidi, Interaction of cations with 2′-deoxythymidine nucleoside and analysis of the nature and strength of cation bonds, Journal of Physical Organic Chemistry 25 (2012) 153-161.

Turkish Computational and Theoretical Chemistry

Turkish Comp Theo Chem (TC&TC)

Volume(Issue): 1(2) – Year: 2017 – Pages: 6-12

ISSN: 2587-1722 / e-ISSN: 2602-3237

Received: 06.05.2017 **Accepted:** 03.07.2017 *Research Article*

Investigating Chitosan–Curcumin Nanorings for Containing Fluorouracil

Hossein Yousefvand [a], Mahmoud Mirzaei [a,1], Majid Tabbakhian [b]

[a] Department of Medicinal Chemistry, School of Pharmacy and Pharmaceutical Sciences, Isfahan University of Medical Sciences, Isfahan, Iran

[b] Department of Pharmaceutics, School of Pharmacy and Pharmaceutical Sciences, Isfahan University of Medical Sciences, Isfahan, Iran

Abstract: Density functional theory (DFT) calculations have been performed to investigate formation possibilities and properties of chitosan–curcumin (Chit–Cur) nanorings for containing fluorouracil (FU) anticancer drug. The B3LYP exchange–correlation functional and the 6–31G* standard basis set have employed for performing DFT calculations. In this case, first, all individual structures have been optimized, then; nanorings have been constructed by the covalent attachments of Chit–Cur counterparts. To this aim, three complexes including FU–Chit2–Cur2, FU–Chit4–Cur2 and FU–Chit6–Cur2 have been constructed by physically locating FU inside the nanorings. The atomic and molecular scales results in isolated gas phase and water solvated systems indicated that the FU–Chit2–Cur2 complex could be expected as a good container for the FU anticancer drug.

Keywords: *Chitosan, Curcumin, Fluorouracil, Nanoring, Density functional theory.*

1. Introduction

Fluorouracil, or 5-fluorouracil, (FU) has been used for several years as an efficient anticancer agent to treat several types of cancers [1]. However, the unwanted side effects made the FU as an unsuitable medicine for the patients [2]. Therefore, several efforts have been dedicated to optimize the usage of FU for the patients with minimum side effects [3]. In this case, designing new carriers to contain and to carry FU until reaching the specific target could be a useful method of modifications of FU usage [4]. Chitosan (Chit) and curcumin (Cur) have been considered as good carriers or complementary materials to carry drugs inside the living systems for some years [5–10]. However, each of Chit and Cur compounds itself may have some deficiencies for the required role of drug carrier [11, 12]. Combining different portions of Chit and Cur together may help to improve the efficiency of using of this material as a better carrier comparing with each individual structure [13]. Solubility is an important task to be considered for carriers, in which it is also important for both of Chit and Cur individual counterparts [14, 15]. In addition to physico–chemical properties, size of carrier is also very much important for the purpose of investigating new drug carriers [16]. After the discovery of nano science and technology, considerable attempts have been done to characterize nano–sized materials for specific

[1] Corresponding author
E-mail: mdmirzaei@pharm.mui.ac.ir;
Mobile: +98–939–4581324

purposes in living systems [17]. Targeted drug delivery systems based on nanostructures have been expected to be very much useful for the purposes of carrying drugs up to the specified targets [18]. In this case, investigations of various types of nanostructures have become one of first aims or researcher of different fields [19]. It is important to note that the nanostructures are such complicated structures to be investigated in the laboratories; therefore, computational chemistry methodologies could help researchers to significantly investigate the formation possibilities and properties of nano based materials [20–22].

Within this work, possibilities of formation for a type of Chit–Cur nanoring to contain FU (Figs. 1 and 2) have been investigated based on density functional theory (DFT) calculations employing the B3LYP exchange–correlation functional and the 6–31G* standard basis set. Optimizations of structural models have been investigated by different numbers of repeating Chit and Cur counterparts. Optimized geometries in addition to atomic/molecular scales properties have been evaluated to achieve the purpose of this work. It is important to note that chemical bonds are used to construct Chit–Cur structures, but FU is kept through physical interactions in the center of constructed nanoring.

2. Computational Method

Within this work, DFT based calculations have been performed employing the standard B3LYP/6–31G* method to investigate formation possibilities and properties for types of Chit–Cur nanorings to contain FU anticancer drug. To achieve this purpose, individual molecular models of Chit, Cur and Fu (Fig. 1) have been firstly optimized to achieve the minimum–energy starting structures to construct hybrid systems. Subsequently, nanorings have been constructed and optimized based on combinations of already optimized Chit and Cur counterparts including Chit2–Cur2, Chit4–Cur2, and Chit6–Cur2 systems (Fig. 2). At the last step, the FU counterpart has been located in the center of nanorings and the complex structures have been optimized again. As a result, there are three individual starting structures: Chit, Cur and FU, three nanorings: Chit2–Cur2, Chit4–Cur2 and Chit6–Cur2, and three complex structures: FU–Chit2–Cur2, FU–Chit4–Cur2, and FU–Chit6–Cur2 (Figs. 1 and 2). The calculations have been performed in two systems of isolated gas phase and water solvated (based on polarizable continuum model, PCM) to obtain molecular and atomic properties. Molecular properties including total energies, binding energies, energies of the highest occupied and the lowest unoccupied molecular orbitals, energy gaps, and dipole moments are summarized in Table 1. Additionally, atomic scale quadrupole coupling constants (QCC) [23] have been calculated for all FU counterparts in the individual and complex forms to see the effects of nanoring on the initial properties of FU (Table 2). It is important to note that QCC parameters are very good elements to investigate the electronic properties of matters [24–26]. These parameters could be obtained by the solid–state nuclear magnetic resonance (NMR) technique, in which reproducing reliable values of QCC is an advantage of computational chemistry [27]. Moreover, it is not easy to perform NMR experiments on the complicated nano systems. All calculations of this work have been performed by the Gaussian 09 program [28].

3. Results and Discussion

3.1 Molecular properties

Within this work, formation possibilities and properties have been investigated for a novel design of Chit–Cur (chitosan–curcumin) nanoring for containing FU (fluorouracil) anticancer (Figs. 1 and 2). To achieve this purpose, the individual structures of Chit, Cur and FU have been optimized to reach to the minimum energy levels. Table 1 presents the results for total energies, HOMO and LUMO energies, energy gaps, and dipole moments for isolated gas phase and water solvated systems. Comparing the results shows that the investigated structures have different properties in both systems. In the next step, Chit and Cur counterparts have been attached together by formation of ether bonds to make possible constructions of Chit–Cur nanorings. As indicated by the results of Table 1, HOMO and LUMO are at different levels of energies for the nanorings with corresponding different energy gaps, in which the values of dipole moments also show different parameters. The value of dipole moment for Chit2–Cur2 is very much highlighted among the three available nanorings (11.889 Debye vs. 4.067 and 6.514 Debye), which

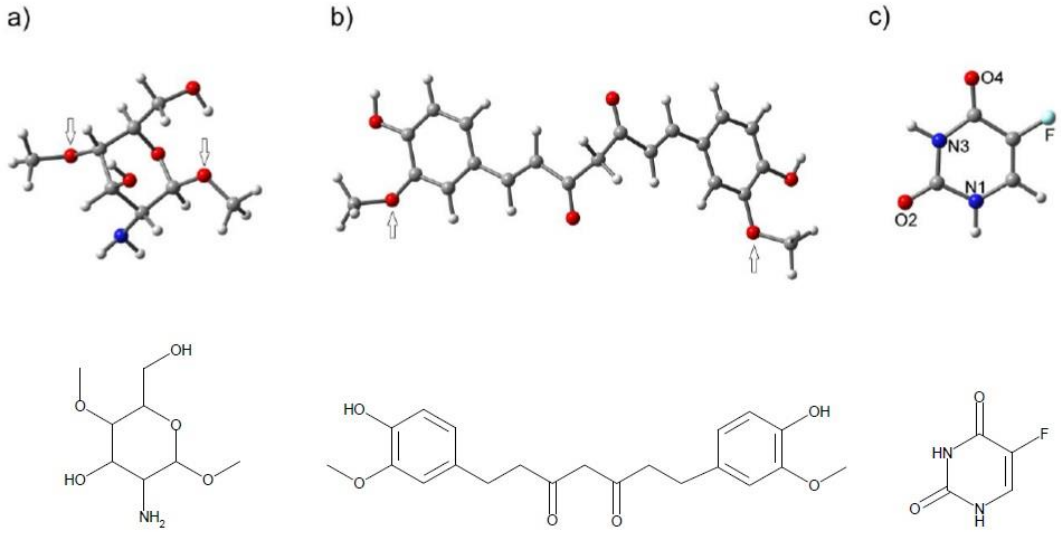

Fig. 1. 3D and 2D views of individual models: a) chitosan (Chit), b) curcumin (Cur), c) fluorouracil (FU). The connecting atomic sites are shown by indicator arrows.

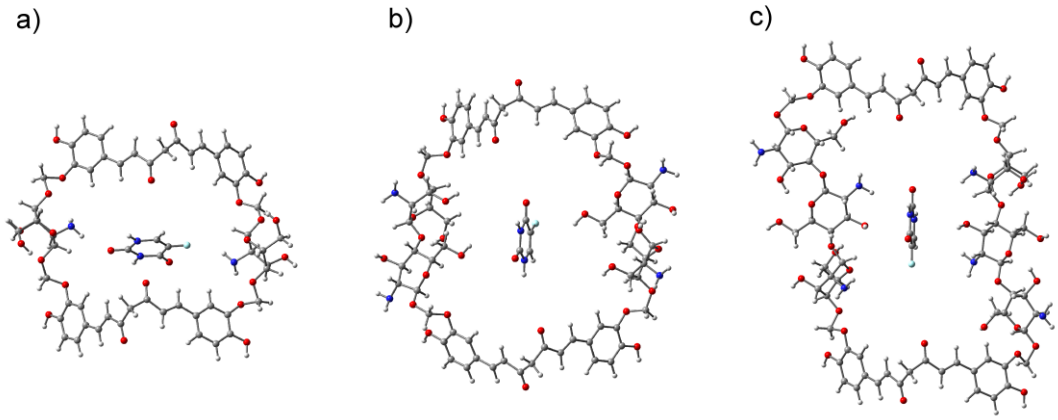

Fig. 2. Complex models: a) FU–Chit2–Cur2, b) FU–Chit4–Cur2, c) FU–Chit6–Cur2.

may refer to more reactivity of this structure than other two ones. At the third step, FU counterparts have been placed at the center of nanorings to construct FU–Chit–Cur complexes. In this case, the values of dipole moments for FU–Chit4–Cur2 and FU–Chit6–Cur2 (4.545 and 7.020 Debye) are increased in comparison with the corresponding Chit–Cur nanorings (4.067 and 6.514 Debye) but the value was decreased for FU–Chit2–Cur2 (8.282 Debye) in comparison with the Chit2–Cur2 nanoring (11.889 Debye). The results of binding energies in both gas and water solvated phases indicate that the most stable complex structure is FU–Chit2–Cur2 among the models (gas phase: 6.190 keV vs. 0.442 and 1.744 keV, water sovlated: 0.871 keV vs. 0.005 and 0.233 keV). It has been already indicated by the values of dipole moments that the reactivity of FU–Chit2–Cur2 could be expected more than other two nanorings, in which it is again confirmed here by the highlighted magnitude of binding energy. Comparing the energies of HOMO and LUMO indicates that the complex structures are more similar to the individual nanorings but not to the individual FU counterparts. Based on the obtained results, the properties of FU and nanorings have been influenced by presenting in the complex systems because of interactions, in which the effects are more significant for the properties of smaller counterpart (FU) than the properties of larger counterpart (nanorings). Earlier studies have been also tried to show the possibility of existence of a

Table 1: Molecular properties*

Model	Total Energy (keV)	HOMO (eV)	LUMO (eV)	Energy Gap (eV)	Dipole Moment (Debye)
Chit	–20.542	–6.323	1.517	7.893	4.907
	[–20.297]	[–6.054]	[2.138]	[8.192]	[6.129]
Cur	–34.384	–5.790	–1.972	3.818	3.833
	[–34.385]	[–5.750]	[–2.023]	[3.727]	[5.121]
FU	–13.988	–6.786	–1.378	5.408	3.902
	[–13.989]	[–6.302]	[0.878]	[7.180]	[5.156]
$Chit_2$–Cur_2	–104.949	–5.611	–1.955	3.656	11.889
	[–104.953]	[–5.618]	[–2.028]	[3.590]	[15.401]
$Chit_4$–Cur_2	–137.107	–5.900	–2.151	3.749	4.067
	[–137.113]	[–5.805]	[–2.050]	[3.755]	[5.668]
$Chit_6$–Cur_2	–169.253	–5.484	–2.146	3.338	6.514
	[–169.259]	[–5.436]	[–2.067]	[3.369]	[7.764]
FU–$Chit_2$–Cur_2	–118.937 (6.190)	–5.622	–2.018	3.604	8.282
	[–118.942 (0.871)]	[–5.616]	[–2.028]	[3.588]	[10.427]
FU–$Chit_4$–Cur_2	–151.096 (0.442)	–5.802	–2.284	3.518	4.545
	[–151.101 (0.005)]	[–5.804]	[–2.053]	[3.751]	[6.349]
FU–$Chit_6$–Cur_2	–183.240 (1.734)	–5.453	–2.135	3.318	7.020
	[–183.247 (0.233)]	[–5.436]	[–2.066]	[3.371]	[7.989]

*See Figs. 1 and 2 for the models. The values in brackets are for the water solvated systems. Energy Gap = LUMO – HOMO. The values in parentheses are for the binding energies (kcal/mol); Binding Energy = $Energy_{\text{FU–Chit–Cur}} - Energy_{\text{Chit–Cur}} - Energy_{\text{FU}}$.

container or carrier for FU counterpart, in which the results are in complementary of each other for the purpose.

Comparing the results of isolated gas phase and water solvated systems indicates the significant effects of solvent on molecular properties of the investigated systems. Total energies of the complex systems indicate that the FU–Chit–Cur structures are slightly more stable in the water solvated system than the isolated gas phase. Binding energies indicate that the solvent could separate the FU counterpart from the nanoring. HOMO and LUMO levels also indicate the effects of solvent on electronic properties of the investigated models, which are also seen by the energy gaps in two systems. Dipole moments significantly show the importance of the investigated complex models with highlighted polarization properties in the water solvated systems. Since the solubility is an important factor for the systems related to life sciences, the results of this work indicated that the designed complex models could help for better solubility activities [1, 3].

3.2 Atomic scale quadrupole coupling constants

Atomic scale QCC (quadrupole coupling constants) parameters have been evaluated for nitrogen and oxygen atoms of FU in the individual and complex models for both isolated gas phase and water solvated systems (Table 2). These two types of atoms of FU are the most important ones, which are the responsible for interactions with other molecules and atoms in the populated systems. Both of nitrogen and oxygen have considerable

quadrupole moments and they are very much active for the QCC measurements [23]. Since the magnitudes of QCC are related to the amounts of electric charges at the atomic sites, larger or smaller values indicate the contribution of the atom to interact with other atoms. For nitrogen atoms, the behaviors in FU–Chit4–Cur2 and FU–Chit6–Cur2 are similar with decrease of magnitude of QCC for both nitrogens from FU to complex. However, behavior in FU–Chit2–Cur2 is different, in which the magnitude of N(3) (3724 kHz) is increased whereas the that of N(1) (4069 kHz) is decreased. Interestingly, the changes of magnitudes of QCC for oxygen atoms from individual FU to FU–Chit2–Cur2 are different in comparison with the situations in the two other complexes. The atomic scale results, in addition to molecular results, also indicate that the properties for FU–Chit2–Cur2 are highlighted among three constructed complexes. In this case, FU–Chit2–Cur2 could be proposed as a good container for the FU counterpart. The effects of solvents on the magnitudes of QCC are also obvious to approve the importance of investigated complex models for better solubility in water systems. Lower magnitudes of QCC in the water solvated systems in comparison with isolated gas phase reveal that the FU counterpart could detect the existence of solvent and could detect the effects.

Table 2: Atomic quadrupole coupling constants (kHz) for fluorouracil*

Model	N_1	N_3	O_2	O_4
FU	4121	3690	8247	9440
	[3768]	[3526]	[8109]	[9060]
FU–Chit$_2$–Cur$_2$	4069	3724	8180	9250
	[3786]	[3533]	[8121]	[9022]
FU–Chit$_4$–Cur$_2$	4076	3656	8292	9495
	[3762]	[3509]	[8114]	[9064]
FU–Chit$_6$–Cur$_2$	4035	3643	8359	9461
	[3748]	[3542]	[8178]	[9066]

*See Figs. 1 and 2 for the atoms and models. The values in brackets are for the water solvated systems.

4. Conclusion

Within this work, formation possibilities and properties have been investigated for FU–Chit–Cur complexes as possible containers for FU anticancer drug in isolated gas phase and water solvated systems. Among the constructed complex models, FU–Chit2–Cur2 has been observed as more possible structure than two other FU–Chit4–Cur2 and FU–Chit6–Cur2 ones. The molecular properties indicated that the reactivity of Chit2–Cur2 nanoring is more than other two Chit4–Cur2 and Chit6–Cur2 nanorings. The magnitudes of binding energies also have approved the expected reactivity for Chit2–Cur2 nanoring. Atomic scale QCC properties indicated that the behaviors of nitrogen and oxygen atoms in the FU–Chit2–Cur2 complex are different in comparison with two other FU–Chit4–Cur2 and FU–Chit6–Cur2 complexes, approving again the highlighted behavior of Chit2–Cur2 nanoring. Therefore, FU–Chit2–Cur2 complex could be proposed as a possible container of FU. The effects of water solvent were also significantly observed for both of molecular and atomic properties. As important achievements of this part, the molecular orbital energy levels and dipole moments indicated the most significant effects. Moreover atomic properties of FU also indicated the effects of solvent, in which the magnitudes of effects are still different for the complex structures. Finally, the constructed containers models could be seen as a possible design for FU related applications, in which the FU–Chit2–Cur2 complex could be proposed as the most proper one among the models.

Acknowledgments

M.M. acknowledges the financial support by the research council of Isfahan University of Medical Sciences (Grant No. 394705).

References

[1] M.A. Safwat, G.M. Soliman, D. Sayed, M.A. Attia, Gold nanoparticles enhance 5-fluorouracil anticancer efficacy against colorectal cancer cells. International Journal of Pharmaceutics 513 (2016) 648-658.

[2] J.K. Kim, K.A. Kang, M.J. Piao, Y.S. Ryu, X. Han, et al., Endoplasmic reticulum stress induces 5-fluorouracil resistance in human colon cancer cells. Environmental Toxicology and Pharmacology 44 (2016) 128-133.

[3] M. Mirzaei, Effects of carbon nanotubes on properties of the fluorouracil anticancer drug: DFT studies of a CNT-fluorouracil compound. International Journal of Nano Dimension 3 (2013) 175-179.

[4] M.M. El-Hammadi, Á.V. Delgado, C. Melguizo, J.C. Prados, J.L. Arias, Folic acid-decorated and PEGylated PLGA nanoparticles for improving the antitumour activity of 5-fluorouracil. International Journal of Pharmaceutics 516 (2017) 61-70.

[5] J.R. Lakkakula, T. Matshaya, R.W.M. Krause, Cationic cyclodextrin/alginate chitosan nanoflowers as 5-fluorouracil drug delivery system. Materials Science and Engineering: C 70 (2017) 169-177.

[6] D.J. Fu, Y. Jin, M.Q. Xie, Y.J. Ye, D.D. Qin, et al., Preparation and characterization of mPEG grafted chitosan micelles as 5-fluorouracil carriers for effective anti-tumor activity. Chinese Chemical Letters 25 (2014) 1435-1440.

[7] C. Gu, V. Le, M. Lang, J. Liu, Preparation of polysaccharide derivates chitosan-graft-poly(ε-caprolactone) amphiphilic copolymer micelles for 5-fluorouracil drug delivery. Colloids and Surfaces B 116 (2014) 745-750.

[8] A. Anitha, N. Deepa, K.P. Chennazhi, Vinoth-Kumar Lakshmanan, R. Jayakumar, Combinatorial anticancer effects of curcumin and 5-fluorouracil loaded thiolated chitosan nanoparticles towards colon cancer treatment. Biochimica et Biophysica Acta – BBA 1840 (2014) 2730-2743.

[9] S.M. Masloub, M.H. Elmalahy, D. Sabry, W.S. Mohamed, S.H. Ahmed, Comparative evaluation of PLGA nanoparticle delivery system for 5-fluorouracil and curcumin on squamous cell carcinoma. Archives of Oral Biology 64 (2016) 1-10.

[10] J. Chen, Z.M. He, F.L. Wang, Z.S. Zhang, X.Z. Liu, et al., Curcumin and its promise as an anticancer drug: An analysis of its anticancer and antifungal effects in cancer and associated complications from invasive fungal infections. European Journal of Pharmacology 772 (2016) 33-42.

[11] Y.O. Jeon, J.S. Lee, H.G. Lee, Improving solubility, stability, and cellular uptake of resveratrol by nanoencapsulation with chitosan and γ-poly (glutamic acid). Colloids and Surfaces B 147 (2016) 224-233.

[12] J. Li, G.H. Shin, W. Lee, X. Chen, H.J. Park, Soluble starch formulated nanocomposite increases water solubility and stability of curcumin. Food Hydrocolloids 56 (2016) 41-49.

[13] Si.B. Subramanian, A.P. Francis, T. Devasena, Chitosan–starch nanocomposite particles as a drug carrier for the delivery of bis-desmethoxy curcumin analog. Carbohydrate Polymers 114 (2014) 170-178.

[14] S.H. Chang, H.T.V. Lin, G.J. Wu, G.J. Tsai, pH Effects on solubility, zeta potential, and correlation between antibacterial activity and molecular weight of chitosan. Carbohydrate Polymers 134 (2015) 74-81.

[15] L. Chen, G. Bai, S. Yang, R. Yang, G. Zhao, et al., Encapsulation of curcumin in recombinant human H-chain ferritin increases its water-solubility and stability. Food Research International 62 (2014) 1147-1153.

[16] M. Azad, J. Moreno, E. Bilgili, R. Davé, Fast dissolution of poorly water soluble drugs from fluidized bed coated nanocomposites: Impact of carrier size. International Journal of Pharmaceutics 513 (2016) 319-331.

[17] R. Gong, G. Chen, Preparation and application of functionalized nano drug carriers. Saudi Pharmaceutical Journal 24 (2016) 254-257.

[18] A. Mokhtarzadeh, M. Tabarzad, J. Ranjbari, M. de la Guardia, M. Hejazi, M. Ramezani, Aptamers as smart ligands for nano-carriers targeting. TrAC Trends in Analytical Chemistry 82 (2016) 316-327.

[19] G. Perret, P. Ginet, M.C. Tarhan, A. Baccouche, T. Lacornerie, et al., Nano

systems and devices for applications in biology and nanotechnology. Solid-State Electronics 115 (2016) 66-73.

[20] D.M. Holland, M.K. Borg, D.A. Lockerby, J.M. Reese, Enhancing nano-scale computational fluid dynamics with molecular pre-simulations: Unsteady problems and design optimization. Computers & Fluids 115 (2015) 46-53.

[21] Bodaghi, M. Mirzaei, A. Seif, M. Giahi, A computational NMR study on zigzag aluminum nitride nanotubes. Physica E 41 (2008) 209-212.

[22] M. Mirzaei, N.L. Hadipour, A. Seif, M. Giahi, Density functional study of zigzag BN nanotubes with equivalent ends. Physica E 40 (2008) 3060-3063.

[23] P. Pyykkö, Spectroscopic nuclear quadrupole moments. Molecular Physics 99 (2001) 1617–1629.

[24] Z. Bagheri, M. Mirzaei, N.L. Hadipour, M.R. Abolhassani, Density functional theory study of boron nitride nanotubes: Calculations of the N-14 and B-11 nuclear quadrupole resonance parameters. Journal of Computational and Theoretical Nanoscience 5 (2008) 614-618.

[25] M. Mirzaei, N.L. Hadipour, A computational NQR study on the hydrogen-bonded lattice of cytosine-5-acetic acid. Journal of Computational Chemistry 29 (2008) 832-838.

[26] M. Mirzaei, F. Elmi, N.L. Hadipour, A systematic investigation of hydrogen-bonding effects on the 17O, 14N, and2H nuclear quadruole resonance parameters of anhydrous and monohydrated cytosine crystalline structures: A density functional theory study. The Journal of Physical Chemistry B 110 (2006) 10991-10996.

[27] T.P. Das, E.L. Han, Nuclear Quadrupole Resonance Spectroscopy, Academic Press, New York, 1958.

[28] M.J. Frisch, G.W. Trucks, H.B. Schlegel, G.E. Scuseria, M.A. Robb, et al., Gaussian 09, Revision A.01, Gaussian Inc.: Wallingford, CT, 2009.

Turkish Computational and Theoretical Chemistry

Turkish Comp Theo Chem (TC&TC)

Volume(Issue): 1(2) – Year: 2017 – Pages: 13-26

ISSN: 2587-1722 / e-ISSN: 2602-3237

Received: 19.05.2017 **Accepted:** 15.06.2017 *Research Article*

Spectroscopic and Quantum Chemical Studies on Some β-Lactam Inhibitors

Sultan Erkan Kariper[1]

Chemistry and Chemical Process Technology, Yıldızeli Vocational School, Cumhuriyet University, Sivas, Turkey

Abstract: Amoxicillin (Amox) and ampicillin (Amp) are investigated by using quantum mechanical methods. These compounds was confirmed by XRD analysis and optimized bond parameters were calculated by density functional (DFT) at B3LYP/6-31G(d) level. The optimized geometrical parameters are in good agreement with crystal data. The experimentally observed FT-IR and NMR picks were assigned to calculated modes for the molecules. Some molecular descriptors are calculated with density functional theory (DFT/B3LYP) 6-31G(d) level in the gas phase. The highest occupied molecular orbital energy (EHOMO), the lowest unoccupied molecular orbital energy (ELUMO), the energy difference (ΔE), hardness (η), softness (σ), electronegativity (χ), chemical potential (μ), electrophilicity index (ω) and nucleophilicity index (ε) are calculated in the this level and associated with inhibition efficiencies of the mentioned β-lactam inhibitors. Molecular Electrostatic Potential (MEP) maps were investigated and predicted the reactive sites. Some quantum chemical descriptors which are total static dipole moment (μ), the average linear polarizability (α), the anisotropy of the polarizability (Δα) and first hyperpolarizability (β) were evaluated for explaining the NLO properties in studies molecules. The inhibition activities were studied using molecular docking studies. The antibiotics were docked into the cocrystallized structure of PXR with SR12813 (PDB ID: 1NRL). Docking results and order of inhibition activity associated with quantum chemical parameters was the same as that of experimental inhibition activity.

Keywords: *β-lactam, DFT, Molecular Docking, Quantum Chemical Parameters.*

Graphical Abstract

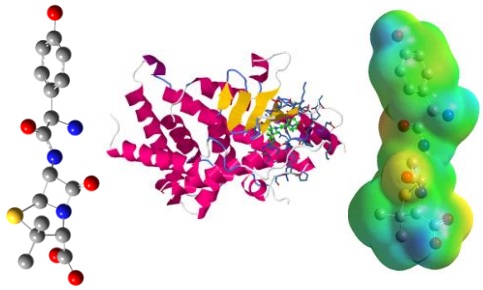

Amoxicillin (Amox) and ampicillin (Amp) were investigated by using quantum mechanical methods. Optimized geometrical parameters, IR and NMR spectroscopic studies were provided for the structure elucidation of chemical species. NLO properties of related molecules are investiggated. Docking was used to predict the bound conformation and binding free energy of small molecules to the target.

[1] Corresponding Author

e-mail: sultanerkan58@gmail.com

1. Introduction

β-lactams have been discovered at the beginning of the twentieth century and they are used in the struggle against pathogenic bacteria [1]. These compounds have the antibacterial effect because they contain amino and carbonyl groups as well as the nitrogen and sulfur atoms in the aromatic structure [2]. In addition, β-lactam antibiotics are applied in the treatment of neurological disorders such as Alzheimer's disease, Parkinson's disease, prion diseases and amyotrophic lateral sclerosis (ALS) [3,4]. Transition metal chelates of β-lactams are effective to prevent the most neurological diseases [5-10].

Amoxicillin (Amox) and ampicillin (Amp) exhibit a similar antibacterial spectrum. Amoxicillin (Amox) and ampicillin (Amp) are two β-lactam antibiotics derivatives. Amox and Amp are effective against both gram-positive and gram-negative organisms which are various pathogenic enteric organisms. Amp is used to infections caused by Escherichia coli, Salmonella, Proteus and Klebsiella [11].

Amox and Amp have not been extensively evaluated in the literature with experimental and theoretical chemistry methods. For this reason, these compounds with vital precautions have been extensively studied, which is spectroscopic behavior and quantum chemical approaches. Density function theory (DFT) is one of the most widely used methods for spectroscopic and quantum chemical studies theoretically in recent years for chemical compounds.

Structural parameters (bond lengths and bond angles) and spectroscopic studies (IR and NMR) provide a basis for the structure elucidation of chemical species. Computational chemistry methods provide visual and detailed analysis of these studies. Non-linear optical (NLO) features have become a very interesting subject due to their potential applications such as optoelectronic devices, optical modulation, molecular switching and optical memory [12]. Therefore, a wide variety of molecular systems inorganic, organic and organometallic were investigated for NLO activity. Some quantum chemical descriptors which are total static dipole moment (μ), the average linear polarizability (α), the anisotropy of the polarizability (Δα) and first hyperpolarizability (β) have been used for explaining the NLO properties in many computational studies. Molecular electrostatic potential (MEP) maps are used to predict the atom with the higher electron density in a molecule. MEP is the potential generated by the charge distribution of a molecule and denotes chemical reactivity, showing nucleophilic and electrophilic sites indicated by MEP maps [13]. For this reason, MEP maps of β-lactam compounds are examined. Molecular descriptors are obtained with quantum chemical calculations. These molecular descriptors are the highest occupied molecular orbital energy (E_{HOMO}), the lowest unoccupied molecular orbital energy (E_{LUMO}), the energy gap (ΔE), hardness (η), softness (σ), electronegativity (χ), chemical potential (μ), electrophilicity index (ω) and nucleophilicity index (ε). Computational docking programs examine interactions with a chemical compound and are widely used for drug discovery and development. Docking is used to predicting the bound conformation and binding free energy of small molecules to the target. Docking Server is a free open source software package for virtual placement of small molecules into macromolecular receptors and developed for making related accounts.

In this study, the studied compounds are optimized at DFT/B3LYP/6-31G(d) level both in the gas phase. The structural parameters are examined and compared with the data obtained from X-rays for Amox and Amp. The computed and experimentally observed spectroscopic values are examined on the β-lactams to give a detailed assignment of the fundamental bands in FT-IR and NMR. The chemical activity areas of the studied compounds are determined via MEP maps. The quantum chemical identifiers are associated with the activities of the compounds. NLO materials have been calculated due to promising applications in optoelectronic technology. For the compounds with the target protein are reviewed to the interacting energies by Molecular Docking studies and are determined to the interaction types and interaction regions.

2. Computational Details

The investigated compounds were drawn with the Gauss View 5.0.8 package program for molecular geometry optimization [14] and the calculation was performed via Gaussian 09 Revision C.01 programme pack (Linux based) in

TÜBİTAK-TR Grid [15]. The calculations included Density Functional Theory (DFT) hybrid B3LYP [16] and used to 6-31G (d) basic sets. Molecular geometries were optimized using B3LYP/6-31G (d) level in the gas phase. IR spectrum was obtained from optimized structures and the frequencies obtained as harmonic were converted to anharmonic frequencies with a scale factor of 0.9600 [17].The proton and carbon NMR chemical shift was calculated with the gauge-including atomic orbital (GIAO) approach by using B3LYP/6-31G(d) level of the studied molecule. Molecular docking (ligand-protein) simulations were performed by using DockingServer free software package.

The total static dipole moment (μ), the mean polarizability (α), the anisotropy of the polarizability (Δα) and the total static first hyperpolarizability (β) using x, y, z components are defined as using Eqs. 1-4 [18].

$$\mu = \left(\mu_x^{\,2} + \mu_y^{\,2} + \mu_z^{\,2}\right)^{1/2} \quad (1)$$

$$a = \frac{1}{3}\left(a_{xx} + a_{yy} + a_{zz}\right) \quad (2)$$

$$\Delta a = \frac{1}{\sqrt{2}}\left[\begin{array}{l}\left(a_{xx} - a_{yy}\right)^2 + \left(a_{yy} - a_{zz}\right)^2 + \\ \left(a_{zz} - a_{xx}\right)^2 + 6a_{xz}^{\,2} + 6a_{xy}^{\,2} + 6a_{yz}^{\,2}\end{array}\right]^{1/2} \quad (3)$$

$$\Delta a = \frac{1}{\sqrt{2}}\left[\begin{array}{l}\left(a_{xx} - a_{yy}\right)^2 + \left(a_{yy} - a_{zz}\right)^2 + \\ \left(a_{zz} - a_{xx}\right)^2 + 6a_{xz}^{\,2} + 6a_{xy}^{\,2} + 6a_{yz}^{\,2}\end{array}\right]^{1/2} \quad (4)$$

According the Koopman's theorem, as can be seen from eq. (5)-(6), Elumo and EHOMO of any chemical species have been associated with its ionization energy and electron affinity values [19-22]

$$I = -E_{HOMO} \quad (5)$$

$$A = -E_{LUMO} \quad (6)$$

Energy gap (ΔE) [23], absolute electronegativity (χ), chemical potential (μ), absolute hardness (η) and absolute softness (σ) are given by eq. (7-11) [24].

$$\Delta E = E_{LUMO} - E_{HOMO} \quad (7)$$

$$\chi = \frac{I+A}{2} \quad (8)$$

$$\mu = -\chi \quad (9)$$

$$\eta = \frac{I-A}{2} \quad (10)$$

$$\sigma = \frac{1}{\eta} \quad (11)$$

Parr et al. have defined electrophilicty index as a measure of energy lowering due to maximal electro flow between donor and acceptor [25].

$$\omega = \frac{\mu^2}{2\eta} \quad (12)$$

Kiyooka et al. have detected that the ω is a function of μ/η in the second-order parabola for various species [26] and they have proposed the ε parameter related to nucleophilicty index.

$$\varepsilon = \mu\eta \quad (13)$$

3. Results and discussion

3.1. Optimized Geometry

The optimized structures of Amox and Amp are shown Figure 1 and the structure parameters (bond length and bond angles) are listed in Table 1 using DFT/B3LYP/6-31G(d) level in the gas phase. The calculated bond lengths are compared with X-ray diffraction data [27]. It can be seen that the results obtained with the calculated values are in agreement with the crystallographic data.

The bond lengths (S-C1, S-C3, C1-C2, C2-N1, N1-C3, N1-C5, C3-C4, C4-C5 and C5-O1) of the Amox and Amp are correlated with X-ray data and R2 values are determined as 0.9756 and 0.9930, respectively. It is shown that the correlation coefficients (R2) close to 1 which provide remarkable data of the theoretical calculations. Therefore, bond lengths which are not in the literature can be foreseen.

Frau et al. investigated the C1-S-C3, C3-N1-C5, O1-C5-N1, C3-N1-C2, C5-N1-C2, C4-C5-N1 and C5-C4-C3 bonds for Amox and compared them with X-ray data. They are given in Table 2 and compared the calculated bond angles with X-ray data.

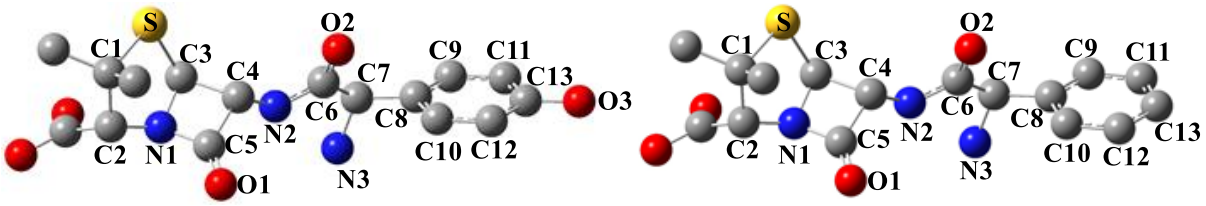

Figure 1. Optimized structure and numbering of Amox and Amp. Hydrogen atoms are not presented for clarity.

Table 1. The calculated and X-ray bond lengths of Amox and Amp

	Amox		Amp	
Bond length	Calc.	X-ray	Calc.	X-ray
S-C1	1.880	1.843	1.881	1.850
S-C3	1.850	1.775	1.851	1.810
C1-C2	1.584	1.559	1.584	1.550
C2-N1	1.443	1.456	1.443	1.460
N1-C3	1.462	1.492	1.462	1.450
N1-C5	1.398	1.381	1.399	1.380
C3-C4	1.571	1.575	1.571	1.530
C4-C5	1.556	1.515	1.556	1.520
C5-O1	1.206	1.200	1.206	1.180
C4-N2	1.427	-	1.427	-
N2-C6	1.369	-	1.369	-
C6-O2	1.222	-	1.222	-
C6-C7	1.547	-	1.546	-
C7-N3	1.546	-	1.481	-
C7-C8	1.518	-	1.521	-
C8-C9	1.401	-	1.399	-
C8-C10	1.401	-	1.402	-
C9-C11	1.392	-	1.396	-
C10-C12	1.393	-	1.394	-
C12-C13	1.399	-	1.397	-
C13-O3	1.367	-	-	-

Table 2. The calculated and X-ray bond angles of Amox and Amp

		Amox	Amp.
Bond angles	Calc.	X-ray	Calc.
C1-S-C3	94.3	90.1	94.3
C3-N1-C5	94.9	93.3	94.9
O1-C5-N1	131.3	131.2	131.3
C3-N1-C2	117.9	117.1	117.9
C5-N1-C2	128.6	127.5	128.6
C4-C5-N1	91.4	93.0	91.4
C5-C4-C3	84.7	85.1	84.8

As a result, R2 value is calculated as 0.991 for Amox. Additionally, bond angles of Amp are given in Table 2, too. The graphs are plotted for Amox and Amp both bond length and bond angle and given in supplementary material. (Supp. Fig. S1). As shown in Table 2, there is a deviation from the ideal geometry at the bond angles of the lactam ring where is the square part and the sulfur ring of the mentioned molecules above. For example, C3-N1-C5, C4-C5-N1 and C5-C4-C3 angles are found as 94.9, 91.4 and 84.7, respectively.

3.2. IR Analysis

A band may consist of multiple vibrational transition in the IR spectrum. Some of the vibrational transitions that form a band are violent and some are weak. Some of the vibrational transitions that form a band are violent and some are weak. Vibrational transition with high severity makes more contribution to band [28]. For this reason, in this study, vibrational transition frequency with the highest intensity in a band was given and all the vibrational movements that make up the band are labeled. The frequencies obtained after the optimization of the molecules are harmonic frequencies and the frequencies obtained experimentally are also anharmonic frequencies. Gaussian calculations provide a scale factor which is converted harmonic frequencies into anharmonic frequencies. The scale factor is 0.9600 of B3LYP method and 6-31G(d) basic set [29]. The vibrational spectra obtained from the optimized structures which calculated at B3LYP/6-31G(d) level in the gas phase of Amox and Amp were given in Figure 2.

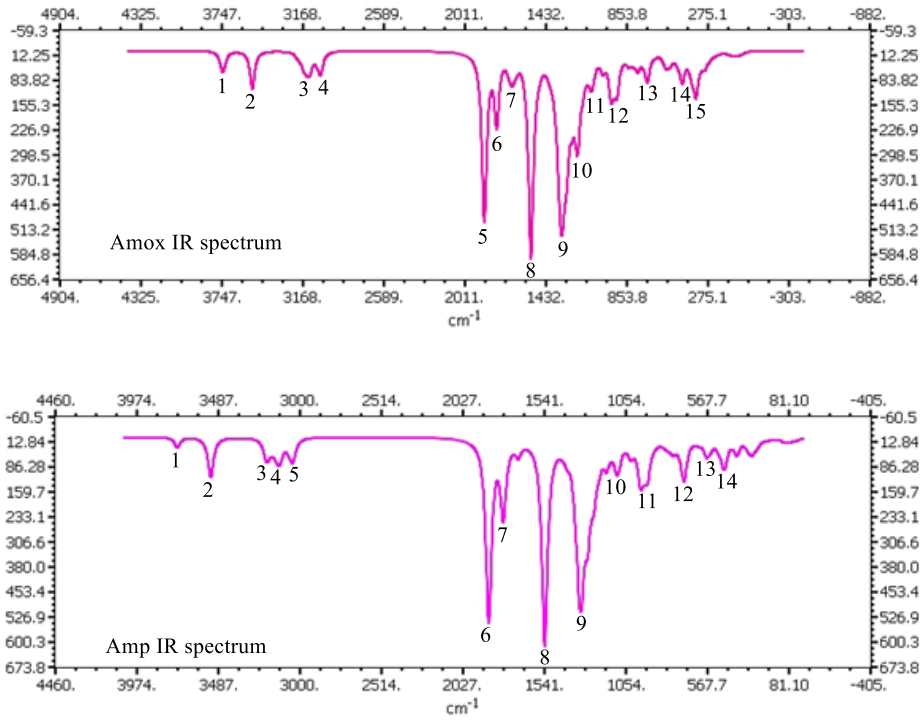

Figure 2. IR spectra of Amox and Amp

As seen in Figure 2, 15 peaks for Amox and 14 peaks for Amp were labeled. Table 3 indicates the anharmonic frequencies for Amox and Amp and the detailed labeling of these vibration modes with obtained at B3LYP/6-31G(d) in the gas phase. According to Table 3, the bond vibrational frequency of the specific OH group of Amox is 3600.1 cm^{-1}. This value in the literature is 3552 cm-1. The N-H vibrational frequency calculated for Amox is 3392.5 cm^{-1} and the experimental frequency is 3161 cm^{-1}. C = O frequency experimentally measured in the β-lactam and amide

region is labeled as 1775 and 1686 cm-1 and the calculated frequencies are found as 1800.7 and 1717.1 cm^{-1}, respectively. Although the experimental value of the N-H bending stretching frequency is 1560 cm^{-1}, the calculated value is determined as 1717.1 and 1481.4 cm^{-1} by an animation program. Observation of other vibrational types besides N-H bending stretching may cause a certain difference between experimental and calculated. The CN bond stretching frequency in the square part is calculated as 1069.9 cm^{-1}, the experimental value of this stretching is 1021 cm^{-1}. The calculated frequency for CS bond stretching is 554.9 cm^{-1} while the experimental stretching is 582 cm^{-1}.

The experimental vibrational frequencies of N-H, C=O of β-lactam and amide region, N-H bending stretching, CN and CS in the Amp are 3200, 1774, 1688, 1516, 1075 and 598 cm^{-1}, respectively. The calculated values for these stretching types are also 3395.1, 1880.8, 1718.8, 1481.6, 1284.4 and 555.6 cm^{-1}. The theoretical and experimental results for some stretching frequencies are very close to each other. Vibration spectroscopy is an effective tool for illuminating the molecular structure and gives a dynamic image of the molecule [30]. The used method and the basic set are chosen quite appropriately for structure verification.

Table 3. Calculated anharmonik frequencies (cm^{-1}) and assignments for Amox and Amp.

	Amox		Amp	
	Anhar. IR	Assign.	Anhar. IR	Assign.
1	3600.1	STRE O-H	3587.3	STRE COO-H
2	3392.5	STRE N-H	3395.1	STRE N-H
3	3005.5	STRE C-H	3072.1	STRE C-H(aro.)
4	2928.1	STRE CH_3	3004.2	STRE C-H
5	1800.7	STRE C=O	2928.5	STRE CH3
6	1717.1	STRE C=O BEND N-H	1800.8	STRE C=O
7	1609.5	STRE C-C(aro.)	1718.8	STRE C=O BEND N-H
8	1481.4	STRE C-N BEND N-H	1481.6	STRE C-N BEND N-H
9	1284.1	STRE C-N BEND C-H	1284.4	STRE C-N (square part) BEND C-H
10	1200.9	STRE C-N BEND C-H BEND N-H	1055.4	STRE C-N BEND C-H BEND N-H
11	1069.9	STRE C-N (square part) BEND C-H	933.1	STRE C-C (square part) Wagging N-H
12	989.5	STRE C-C TORS CH_3	686.4	OUT C-H (aro.)
13	682.5	OUT N-H	555.6	STRE C-S
14	554.9	STRE S-C	458.0	OUT O-H
15	349.5	Wagging O-H		

STRE; bond stretching, BEND; valence angle bending, OUT; out-of-plane bending and Wagging; valence angle bending between the planes.

3.3. NMR spectral analysis

Nuclear magnetic resonance (NMR) spectroscopy is one of the most frequently used methods in structure illumination. The chemical shift values for the ^{13}C and ^{1}H-NMR of the investigated compounds are given in Tables 3 and 4. Experimental ^{13}C and ^{1}H-NMR spectra of t' compounds were obtained in the DMSO-d_6+Na 18 in the D2O solvent [31]. Theoretical NMR spectra were calculated in the gas phase. Theoretical 13C and 1H NMR chemical shifts are presented in Tables 3 and 4 with reference to TMSO using the GIAO method [32] in the gas phase for the optimized structures obtained at the B3LYP/6-31G(d) level. The atomic labeling of the mentioned compounds for NMR data is indicated in Figure 3. The results of Table 3 and 4 show that the theoretical chemical shifts obtained by the DFT method are in good agreement with experimental data. The chemical shift values, which are slightly different from the experimental value, arising from the theoretical calculations taking place in isolated gas phase.

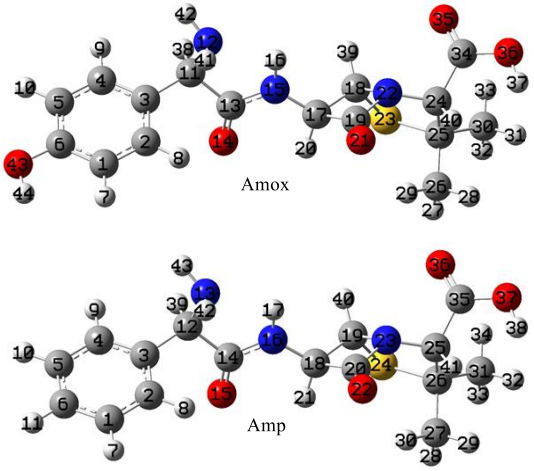

Figure 3. Labeling atomic number of Amox and Amp.

According to Table 3, 13C-NMR the chemical shift value of 6C for the Amox compound is greater than the chemical shift value of other carbons in the ring. Likewise, the chemical shift values of 13C, 19C and 34C for the compound are higher than the chemical shift values of the other carbons. This is a theoretically expected situation. Because the electronegative oxygen atom attracts more electrons from the carbon atoms it is bound to. In this case, the nuclei of these carbon atoms show less shielding effect. Less shielded nuclei show the higher chemical shift. The similar situation is valid for Amp compound in Table 3 and the hydrogen atoms in Table 4.

Computational studies have many advantages. Experimental NMR does not give the chemical shift value separately for atoms and the atoms with similar chemical structure entities have similar values. However, theoretical calculations give the value of individual chemical shifts for each atom and also illuminate many chemical shift values that are not observed experimentally.

Table 3. ^{13}C-NMR data of Amox and Amp

	Amox			Amp	
Atoms	Calc.	Exp.	Atoms	Calc.	Exp.
1C	107.9	115.0	1C	122.7	127.0
2C	122.3	131.4	2C	120.6	128.5
3C	128.1	128.1	3C	136.8	127.0
4C	124.5	131.4	4C	122.3	128.5
5C	108.5	115.0	5C	121.6	127.0
6C	147.5	156.8	6C	120.6	127.5
11C	61.1	57.2	12C	61.8	57.0
13C	159.4	173.1	14C	159.3	174.0
17C	67.3	57.5	18C	67.3	57.7
18C	76.6	67.0	19C	76.6	67.1
19C	161.3	170.0	20C	161.4	171.0
24C	68.8	73.9	25C	68.8	74.0
25C	70.1	64.6	26C	70.3	65.0
26C	34.5	31.8	27C	34.4	31.0
30C	25.7	27.5	31C	25.6	27.5
34C	156.1	173.6	35C	156.2	174.2

Table 4. ^{1}H-NMR data of Amox and Amp

	Amox			Amp	
Atoms	Calc.	Exp.	Atoms	Calc.	Exp.
7H	6.11	6.75	7H	7.23	7.45-7.31
8H	6.90	7.22	8H	7.04	7.45-7.31
9H	6.85	8.50	9H	6.90	7.45-7.31
10H	6.61	8.50	10H	7.16	7.45-7.31
16H	7.83	n.o.	11H	7.16	7.45-7.31
20H	5.37	5.45	17H	7.79	7.56
27H	1.59	1.49	21H	5.40	5.42
28H	1.23	1.49	28H	1.60	1.50
29H	1.65	1.49	29H	1.23	1.50
31H	1.15	1.59	30H	1.66	1.50
32H	1.64	1.59	32H	1.16	1.56
33H	1.66	1. 59	33H	1.64	1.56
37H	5.30	-	34H	1.67	1.56
38H	3.95	4.53	38H	5.31	-
39H	5.23	5.41	39H	3.93	4.54

40H	3.71	3.98	40H	5.25	5.46
41H	0.32	-	41H	3.71	3.97
42H	1.22	-	42H	0.40	n.o.
44H	3.48	n.o.	43H	1.27	n.o.

n.o. not observed.

3.4. Quantum chemical parameters

The molecular descriptors were calculated by using B3LYP/6-31G(d) level for investigation of inhibition efficiencies of β-lactam inhibitors given in Figure 1. The calculated molecular descriptors were given in Table 5 at gas phase. Abdallah experimentally identified the biological activities of these compounds and found that the inhibitory activity of Amox was greater than Amp [33].

Table 5. Quantum chemical parameters with B3LYP/6-31G(d) level in gas phase of inhibitors

Parameters	Amox	Amp
E_{HOMO}*	-5.962	-6.271
E_{LUMO}*	-0.414	-0.414
ΔE	5.549	5.857
η	2.774	2.928
σ	0.360	0.341
χ	3.188	3.343
μ	-3.188	-3.343
ω	1.832	1.908
ε	-8.845	-9.789

*E_{HOMO} and E_{LUMO} are given in eV unit

E_{HOMO} is a parameter associated with the electron donating ability of molecule [34,35]. If the E_{HOMO} increases, electron transfer tendency will increase to the LUMO of appropriate receptor molecules. The molecule having the higher E_{HOMO} indicates the higher inhibition effect. The order of the calculated E_{HOMO} values for these compounds is:

Amox >Amp

E_{LUMO} is a measure of electron accepting ability of chemical species. E_{LUMO} determines the polarizability of the compound i.e. the ability to be distorted by an electric field, and hence LUMO level receives electrons. Experimental and theoretical studies related to biological activity show that increasing of E_{LUMO} decreases the corrosion activities of molecules. Exchange of the calculated E_{LUMO} values for these compounds is:

Amox = Amp

The separation energy, ΔE is an important parameter as a function of reactivity of the molecule and chemical hardness is defined as resistance to electron transfer. The larger values of the HOMO-LUMO energy gap and chemical hardness will provide low reactivity for chemical species. The inhibition efficiencies orders according to ΔE gap and η will be similar to each other. The rankings of the ΔE and η values are:

Amox <Amp

Softness is the inverse of chemical hardness and represents high reactivity. Therefore, soft molecules exhibit high electron donating tendency and high biological activity effect. Exchange of the calculated σ values for these compounds is:

Amox >Amp

Absolute electronegativity is taken into account as a chemical descriptor in comparison of inhibition effects of chemical species. It should be noted that strong inhibitors should have low electronegativity values. Because inhibitors with low electronegativity are tended to give the electron. For a reaction of two systems with different electronegativity the electronic flow will occur from the molecule with the lower electronegativity towards that of higher value until the chemical potentials are equal [36,37]. The ranking of χ values for these compounds is:

Amox <Amp

Chemical potential is the inverse of the electronegativity. Therefore, the inhibition efficiency increases with increasing of chemical potential. Chemical hardness and softness, chemical potential are known as global reactivity descriptors [38]. According to the chemical potential, the inhibitor efficiency ranking should be:

Amox >Amp

Recently, Parr et al. have defined a new descriptor [39]. This parameter is a numeric expression of the global electrophilic power of the molecule that known as electrophilicity index (ω).

The electrophilicity index is a descriptor that represents the reactivity of the chemical species. The global electrophilicity index of the molecule allows quantitative classification of its reactive [40-44]. The electrophilicity index shows the ability of the electron-accepting ability [45]. According to the electrophilicity index, the inhibitor efficiency ranking should be:

Amox <Amp

Nucleophilicity index indicates the electron-donating ability of inhibitor molecules. The inhibition efficiency increases with increasing the ε value or decreasing the ω value. According to the nucleophilicity index, the inhibitor efficiency ranking should be:

Amox >Amp

If inhibitory activities in terms of the molecular properties of the β-lactam compounds are examined, this inhibitory efficiency rankings are an expected result. Amox among the first group of inhibitors are expected the condition to have higher inhibitory efficiency. The phenyl ring has a negative inductive effect. Moreover, OH group on the phenyl ring at Amox provides form stable complexes of compounds because it increases the electron density in the ring. Thus, localization of the electron pairs on the nitrogen atom of the NH_2 group increases. In this case, inhibitory efficiency increases of these molecules.

3.5. Molecular Electrostatic Potential (MEP) Maps

Molecular electrostatic potential (MEP) maps are used to predict the atom with the higher electron density in a molecule. MEP is the potential generated by the charge distribution of a molecule and denotes chemical reactivity, showing nucleophilic and electrophilic sites indicated by MEP contour maps [46]. For the consideration of the reactive behavior of a chemical system and to investigate the molecular structure with its physiochemical property relationships, the three-dimensional distribution of its MEP is helpful [47]. In MEP diagram negative regions can be regarded as nucleophilic centers [48]. Negative electrostatic potential corresponds to the attraction of a proton by the concentrated electron density in the molecule (lone pairs, pi-bonds); thus, revealing sites for electrophilic attack (colored in shades of red in standard contour diagrams) Positive electrostatic potential corresponds to the repulsion of a proton by the atomic nuclei in regions where low electron density exists and the nuclear charge is incompletely shielded (colored in shades of blue in standard contour diagrams) [49]. Theoretical methods can be used to answer these questions that may be greatly helpful in designing other and better drugs. Molecular electrostatic potentials (MEP) computed using ab initio methods can be particularly useful in this context since MEP is known to be a reliable descriptor of hydrogen bonding [50–55].

The MEP maps of inhibitors which calculated B3LYP/6-31G(d) are given in Figure 4. The third region with higher electron density is labeled in maps. These regions are referred to as Zone 1, Zone 2 and Zone 3. According to this diagram will be protonated regions. Zone 1,2 and 3 have protonated region for Amox (14, 21 and 35O), Amp (15, 22 and 36O). As a result, the MEP map show that the negative potential region is on oxygen atom which is the biologically active region.

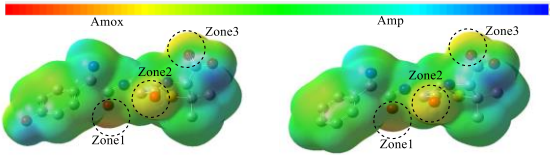

Figure 4. The MEP maps of the neutral inhibitor molecules at HF/6-31++G(d,p) level in gas phase

3.6. Non-Linear Optical (NLO) Properties

NLO is important property in providing the key functions of frequency shifting, optical modulation, optical switching, optical logic and optical memory for the technologies in areas such as telecommunications, signal processing and optical interactions [10]. In the recent studies, NLO is attracted a lot of attention. Organic molecules exhibit significantly NLO properties due to delocalized π electron moving along the molecule. NLO materials are categorized as semiconductor multilayer structures. Therefore, a wide variety of molecular systems inorganic, organic and organometallic were investigated for NLO activity. Some quantum chemical descriptors which are total static dipole moment (μ), the average linear polarizability (α), the anisotropy of the polarizability (Δα) and first hyperpolarizability (β)

have been used for explaining the NLO properties in many computational studies. NLO properties and urea is taken according to standards were calculated at the DFT/B3LYP/6-31G(d) level for the studied ligand. These parameters are given in Table 6.

Table 6 The calculated dipole moment (μ), average linear polarizability (α), the anisotropy of the polarizability (Δα) and hyperpolarizability (β) for urea and investigated molecules.

	μ(D)	α/(Å^3)	Δα/(Å^3)	β_0 (cm^5/esu)x10^{-30}
Urea	1.8059	2.0958	8.8780	297.3869
Amox	1.1490	23.4659	58.9546	2539.9904
Amp	0.5947	25.4659	66.6607	938.9493

NLO properties can be affected from polarizability, the anisotropy of the polarizability and hyperpolarizability. NLO properties increase with increasing the linear polarizability, the anisotropy of the polarizability and first hyperpolarizability. According to Table 3, all values of each mentioned molecules are greater than their urea values. Therefore, NLO properties of Amox and Amp are better than urea and these molecules can be used as NLO material [56].

3.7. Molecular Docking Study

Molecular docking is an effective tool used to achieve binding affinity between the identified ligand and the appropriate target protein of this ligand. Docking is a program that is allowed to interact with a chemical known as a 'receptor' and a chemical entity known as a 'ligand' in a software to analyze interactions between the receptor and ligand. The interaction can be analyzed by evaluating various parameters such as the free energy of binding (kcal/mol). Binding energy is a measure of the affinity of the ligand-protein complex [57]. As the energy decreases, the stability of the complex increases. Computational approaches can be a method for filtering molecules before the experimental test. Docking methods may need a combination with other computational methods for structure-activity relationships [58].

The starting structure was selected by PDB Database (PDB ID: 1NRL) for Amox and Amp and the molecular docking calculations were performed on AutoDock [59] is a free open source software package for virtual placement of small molecules into macromolecular receptors and developed for making related accounts. For this reason, all ligands were studied in the docking program with this target protein. The interaction between the ligands and the target enzyme are presented in the Figure 5.

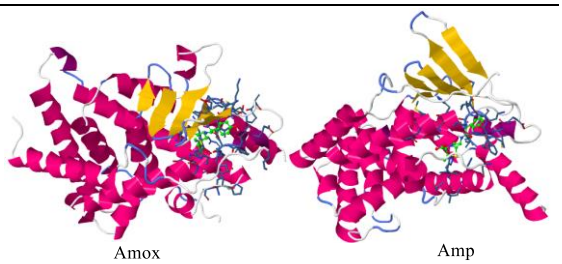

Figure 5. Ligands (green balls) interaction with protein 2J9N.

According to molecular docking result, interaction energies that occur when ligands bind to the protein for Amox and Amp is -9.0 and -8.29 kcal/mol, respectively. These results show that the inhibition efficiency of Amox is higher than Amp. Ki provides information that predicts that a ligand can inhibit an enzyme and interact with a substrate for the enzyme. Docking server inhibition constant for Amox and Amp is 229.81 and 837.77 nM, respectively. If Ki is smaller, less drug is needed to inhibit the enzyme activity and this situation shows that the ligands are within reasonable limits [60]. If vdW is hydrogen bond and dissolved energy is negative, the ligand is well attached to an active site on the target molecule. Similarly, if the electrostatic energy is negative, this negative value proves that the ligands are linked to the target molecule [61]. These values in the molecular docking results are negative for the ligands. So, it can say it is appropriate for the selected target molecule ligands. In accordance with the docking server which gives the binding site analysis, the ligands interacted well with the protein in the docking grid.

The hydrogen bond between Amox and 1NRL is between the nitrogen atoms of the ligand and LEU209 and SER238 of the target proteins. Polar bonds are between the hydrogen atom of the ligand SER238. There are hydrophobic bonds between the carbon atoms in the ligand and LEU206, LEU209, PRO227, LEU239, MET243, HIS407 and ILE414.

The hydrogen bonds for Amp are between nitrogen atoms LEU209. Polar bonds are between oxygen atoms and SER247. π-π interactions occur between the carbon atoms of the ligand and HIS407. The hydrophobic interactions of this ligand exist between the carbon atoms and LEU239, LEU240, MET243 and LEU411. According to molecular docking calculations, the most important interaction is the hydrogen bond interaction. Amox has made more H-bonds than Amp. As a result, according to experimental, theoretical and docking studies, Amox is a molecule with a higher inhibitory activity than Amp.

4. Conclusion

Amoxicillin (Amox) and ampicillin (Amp) were calculated at B3LYP/6-31G(d) level. The optimized geometrical parameters are in good agreement with crystal data. The theoretical and experimental results for some strecthing frequencies are very close to each other. It was observed that the theoretical chemical shifts obtained by the DFT method were in good agreement with the experimental data and it was thought that the difference between the experimental values and the calculated chemical shift values was derived from the theoretical calculations in the isolated gas phase. The biological activity suggested from the quantum chemical parameters and the experimental induction activities gave very similar results for the molecules. MEP maps for Amox and Amp show that the biologically active region is on the oxygen atom. NLO properties of Amox and Amp are better than urea and these molecules can be used as NLO material. As a result, according to experimental, theoretical and docking studies, Amox is a molecule with a higher inhibitory activity than Amp.

Acknowledgment

This research was made possible by TUBITAK ULAKBIM, High Performance and Grid Computing Center (TR-Grid e-Infrastructure).

References

[1] John D. Buynak. Understanding the longevity of the b-lactam antibiotics and of antibiotic/b-lactamase inhibitor combinations. Biochemical pharmacology, 71(2006)930 – 940.

[2] Gökhan Gece, Drugs: A review of promising novel corrosion inhibitors, Corrosion Science, 53 (2011) 3873–3898

[3] M.S. Forman, J.Q. Trojanowski, V.M-Y. Lee, Neurodegenerative diseases: a decade of discoveries paves the way for therapeutic breakthroughs, Nat. Med., 10 (2004) 1055–1063.

[4] J.D. Rothstein, S. Patel, M.R. Regan, C. Haenggeli, Y.H. Huang, D.E. Bergles, L. Jin, M.D. Hoberg, S. Vidensky, D.S. Chung, S.V. Toan, L.I. Bruijn, Z.Z. Su, P. Gupta, P.B. Fisher, b-Lactam antibiotics offer neuroprotection by increasing glutamate transporter expression, Nature, 433 (2005) 73–77.

[5] K.J. Barnham, C.L. Masters, A.I. Bush, Neurodegenerative diseases and oxidative stress, Nat. Rev. Drug Discov., 3 (2004) 205–214.

[6] J.S. Valentine, P.J. Hart, Bioinorganic chemistry special feature: misfolded CuZnSOD and amyotrophic lateral sclerosis, Proc. Natl. Acad. Sci. USA, 100 (2003) 3617–3622.

[7] M. Azzouz, P. Poindron, S. Guettier, N. Leclerc, C. Andres, J.M. Warter, J. Borg, Prevention of mutant SOD1 motoneuron degeneration by copper chelators in vitro, J. Neurobiol., 42 (2000) 49–55.

[8] A. Sher, M. Veber, M. Marolt-Gomisˇcˇek, Spectroscopic and polarographic investigations: copper (II)–penicillin derivatives, Int. J. Pharm., 148 (1997) 191–199.

[9] A. Sher, M. Veber, M. Marolt-Gomiscek, S. Gomiscek, The study of complexation of copper(II) with ampicillin. I. Spectroscopic and electrochemical investigations of interactions at equilibrium conditions, Int. J. Pharm., 90 (1993) 181–186.

[10] G. Mukherjee, T. Ghosh, Metal ion interaction with Penicillins. Part VII: Mixed-ligand complex formation of cobalt(II), nickel(II), copper(II), and Zinc(II) with ampicillin and nucleic bases, J. Inorg. Biochem. 59 (1995) 827–833.

[11] Valentina Gamba, Guglielmo Dusi, Liquid chromatography with fluorescence detection of amoxicillin and ampicillin in feeds using pre-column derivatization, Analytica Chimica Acta, 483 (2003) 69–72.

[12] Şirin Bitmez, Koray Sayin, Bariş Avar, Muhammet Köse, Ahmet Kayraldız, Mükerrem Kurtoğlu, Preparation, spectral, X-ray powder diffraction and computational studies and genotoxic properties of new azo–azomethine metal chelates, 1076 (2014) 213–226.

[13] P. Politzer, D.G. Truhlar, Chemical Applications of Atomic and Molecular Electrostatic Potentials. Academic Press, New York, 1981.

[14] A. Bergamo, G. Sava, Dalton Trans., 40 (2011) 7817-7823.

[15] C. G. Hartinger, M. A. Jakupec, S. Zorbas-Seifried, M. Groessl, A. Egger, W. Berger, H. Zorbas, P. J. Dyson, B. K. Keppler, Chem. Biodiversity, 5 (2005) 2140-2154.

[16] Mohamed K. Awad, Mohamed R. Mustafa, Mohamed M. Abo Elnga, Computational simulation of the molecular structure of some triazoles as inhibitors for the corrosion of metal surface, Journal of Molecular Structure: THEOCHEM, 959 (2010) 66–74.

[17] Jeffrey P. Merrick, Damian Moran, Leo Radom, An Evaluation of Harmonic Vibrational Frequency Scale Factors, J. Phys. Chem., A 2007, 111, 11683-11700.

[18] D. Sajan, J. Hubert, V.S. Jayakumar, J. Zaleski, J. Mol. Struct., 785 (2006) 43–53.

[19] T. Koopmans, Physica, 1 (1933) 104

[20] S. Kaya, S. Erkan Kariper, A. Ungördü, C. Kaya, Effect of Some Electron Donor and Electron Acceptor Groups on Stability of Complexes According to the Principle of HSAB, Journal of New Results in Science, 4 (2014) 82-89.

[21] D.B. Alexander, A.A. Moccari, Evaluation of corrosion inhibitors for component cooling water systems, Corrosion Science., 49 (1993) 921–928.

[22] V.S. Sastri, J.R. Perumareddi, Corrosion, 53 (1996) 671.

[23] W. Kohn, L.J. Sham, Quantum density oscillations in an inhomogeneous electron gas, Physical Review, 137 (1965) A1697–A1705.

[24] R.G. Pearson, Inorg. Chem., 27 (1988) 734.

[25] R. G. Parr, V.Szentpaly, S. Liu, J.Amc. Chem. Soc., 121(1999) 1922

[26] S. Kiyooka, D. Kaneno, R. Fujiyama, Tetrahedron Letters, 54 (2013) 339.

[27] Koray Sayin, Duran Karakas, Nihat Karakus, Tuba Alagöz Sayin, Zinet Zaim, Sultan Erkan Kariper, Spectroscopic investigation, FMOs and NLO analyses of Zn(II) and Ni(II) phenanthroline complexes: A DFT approach, Polyhedron, 90 (2015) 139–146.

[28] http://cccbdb.nist.gov/vibscalejust.asp

[29] D. Rajaraman, G. Sundararajan, N.K. Loganath, K. Krishnasam, Synthesis, molecular structure, DFT studies and antimicrobial activities of some novel 3-(1-(3,4-dimethoxyphenethyl)-4,5-diphenyl-1H-imidazol-2-yl)-1H-indole derivatives and its molecular docking studies, Journal of Molecular Structure, 1127 (2017) 597-610.

[30] R. Di Stefano, M. Scopelliti, C. Pellerito, T. Fiore, R. Vitturi, M.S. Colomba, P. Gianguzza, G.C. Stocco, M. Consiglio, L. Pellerito, Organometallic complexes with biological molecules XVII. Triorganotin(IV) complexes with amoxicillin and ampicillin, Journal of Inorganic Biochemistry, 89 (2002) 279–292.

[31] R. Ditchfield, Molecular orbital theory of magnetic shielding and magnetic susceptibility, J. Chem. Phys., 56 (1972) 5688-5692.

[32] M. Abdallah, Antibacterial drugs as corrosion inhibitors for corrosion of aluminium in hydrochloric solution. Corrosion Science, 46 (2004) 1981–1996.

[33] D.B. Alexander, A.A. Moccari, Evaluation of corrosion inhibitors for component cooling water systems, Corrosion, 49 (1993) 921–928.

[34] A.J. LopesJesus, Luciana I.N. Tomé, M. Ermelinda, S. Eusébio, Mário T.S. Rosado, J.S. Redinha, Hydration of cyclohexylamines: CPCM calculation of hydration gibbs energy of the conformers, Journal of Physical Chemistry A, 111 (2007) 3432–3437.

[35] P. Udhayakala, A. Maxwell Samuel, T. V. Rajendiran and S. Gunasekaran, Quantum chemical study on inhibitory action of some

substituted 1,3,4-oxadiazoles on mild steel, Der Pharmacia Lettre, 5 (2013) 272-283.

[36] Martınez S, Mater Chem and Phys., 77(2002) 97-102.

[37] R. Parthasarathi, V. Subramanian, D. R. Roy and P. K. Chattaraj, Electrophilicity index as a possible descriptor of biological activity, Bioorganic & MedicinalChemistry, 12 (2004) 5533–5543.

[38] R. G. Parr, V.Szentpaly, S. Liu, J.Amc. Chem. Soc., 121 (1999) 1922.

[39] Parthasarathi, R.; Padmanabhan, J.; Subramanian, V.; Maiti, B.; Chattaraj, P. K. J. Phys. Chem. A, 107 (2003) 10346.

[40] Thanikaivelan, P.; Subramanian, V.; Raghava Rao, J.; Nair, B. U. Chem. Phys. Lett., 323 (2000) 59.

[41] Parthasarathi, R.; Padmanabhan, J.; Elango, M.; Subramanian, V.; Chattaraj, P. K. Chem. Phys. Lett., 394 (2004) 225.

[42] Parthasarathi, R.; Padmanabhan, J.; Subramanian, V.; Maiti, B.; Chattaraj, P. K. Curr. Sci., 86 (2004) 535.

[43] Parthasarathi, R.; Padmanabhan, J.; Subramanian, V.; Sarkar, U.; Maiti, B.; Chattaraj, P. K. Internet Electron J. Mol. Des., 2 (2003) 798.

[44] N.O. Obi-Egbedi, I.B. Obot, M.I. El-Khaiary, Quantum chemical investigation and statistical analysis of the relationship between corrosion inhibition efficiency and molecular structure of xanthene and its derivatives on mild steel in sulphuric acid, Journal of Molecular Structure, 1002 (2011) 86-96.

[45] P. Politzer, D.G. Truhlar, Chemical Applications of Atomic and Molecular Electrostatic Potentials. Academic Press, New York, 1981.

[46] M. Wagener, J. Sadowysky, J. Gasteiger, J. Am. Chem. Soc., 117 (1995) 7769–7775.

[47] Jayaraman Jayabharathi, Venugopal Thanikachalam, Marimuthu Venkatesh Perumal, Natesan Srinivasan, Fluorescence resonance energy transfer from a bio-active imidazole derivative 2-(1-phenyl-1H-imidazo[4,5-f][1,10]phenanthrolin-2-yl)phenol to a bioactive indoloquinolizine system, Spectrochimica Acta Part A, 79 (2011) 236–244.

[48] G.C. Muscia, Synthesis trypanocidal activity and molecular modeling studiesof 2-alkylaminomethylquinoline derivatives, European Journal of Medicinal Chemistry, 46 (2011) 3696-3703.

[49] P.S. Kushwaha, P.C. Mishra, Int. J. Quant. Chem., 76 (2000) 700.

[50] A. Kumar, C.G. Mohan, P.C. Mishra, J. Mol. Struct. (Theochem), 361 (1996) 135.

[51] C. Santosh, P.C. Mishra, J. Mol. Model, 3 (1997) 172.

[52] P.C. Mishra, A. Kumar, J.S. Murray, K.D. Sen (Eds.), Molecular Electrostatic Potentials: Concepts and Applications, Theoretical and Computational Chemistry Book Series, Elsevier, Amsterdam, 3 (1996) 257.

[53] A.K. Singh, P.S. Kushwaha, P.C. Mishra, Int. J. Quant. Chem., 82 (2001) 299.

[54] M.K. Shukla, P.C. Mishra, J. Mol. Struct. (Theochem), 340 (1995) 159.

[55] Muhammet Kose, Ceylan Hepokur, Duran Karakas, Vickie McKee, Mukerrem Kurtoglu, Structural, computational and cytotoxic studies of square planar copper(II) complexes derived from dicyandiamide, Polyhedron, 117 (2016) 652–660.

[56] Ramchander Merugu, Uttam Kumar Neerudu, Karunakar Dasa, Kalpana V. Singh, Molecular docking studies of deacetylbisacodyl with intestinal sucrase-maltase enzyme, International Journal of Advances in Scientific Research, 2 (2016) 191-193.

[57] Sugio S, Kashima A, Mochizuki S, Noda M, Kobayashi K. Crystal structure of human serum albumin at 2.5 Aresolution. Protein Eng.,12 (1999) 439-46.

[58] Khandelwal A, Krasowski MD, Reschly EJ, Sinz M, Swaan PW and Ekins S Machine learning methods and docking for predicting human pregnane X receptor activation. Chem Res Toxicol, (2008).

[59] Ramchander Merugu, Uttam Kumar Neerudu, Karunakar Dasa, Kalpana V. Singh, Molecular docking studies of deacetylbisacodyl with intestinal sucrase-maltase enzyme, International Journal of Advances in Scientific Research, 2 (2016) 191-193.

[60] Dipita Bhakta, Ramamoorthy Siva, Morindone, an Anthraquinone, Intercalates DNA Sans Toxicity: a Spectroscopic and Molecular Modeling Perspective, Appl Biochem Biotechnol 167 (2012) 885–896.

Turkish Computational and Theoretical Chemistry

Turkish Comp Theo Chem (TC&TC)

Volume(Issue): 1(2) – Year: 2017 – Pages: 27-34

ISSN: 2587-1722 / e-ISSN: 2602-3237

Received: 11.11.2017 ***Accepted:*** 29.11.2017 *Research Article*

Benchmark Study of The Exchange-Corrected Density Functionals: Application to Strained Boron Nitride Clusters

N.V. Novikov [a], I.Y. Dolinskiy [a], M.A. Gimaldinova [a], K.P. Katin [a,b,1], M.M. Maslov [a,b]

[a] Department of Condensed Matter Physics, National Research Nuclear University MEPhI, Kashirskoe Sh. 31, Moscow 115409, Russia

[b] Laboratory of Computational Design of Nanostructures, Nanodevices and Nanotechnologies, Research Institute for the Development of Scientific and Educational Potential of Youth, Aviatorov Str. 14/55, Moscow 119620, Russia

Abstract: We present a quantum chemical study of three small boron nitride clusters B_2N_2, B_3N_3 and B_4N_4. Their structure and electronic characteristics are calculated by means of the coupled cluster (CC) and density functional theory (DFT) techniques. In order to find the best match with the coupled cluster data the twenty-four DFT exchange-corrected functionals are analyzed. According to our results, B3P86V5 and B97 functionals reproduce well the geometry of small boron-nitrides, whereas for the electronic characteristics OP and VWN functionals give the closest to CC results. Note that prevalent B3LYP and PBE0 DFT-functionals demonstrate lower accuracy.

Keywords: *coupled cluster, density functional theory, exchange-corrected functionals, boron nitride clusters, boron nitride cubane.*

1. Introduction

After discoveries of fullerenes, nanotubes and graphene, many novel carbon architectures were proposed and investigated. They include peapods [1], fullerites [2], diamonds [3,4], and many others [5-8]. In these structures, carbon atoms form k-membered cycles, in which k value varies mostly from 4 to 8. Note, that only a limited number of high-strained structures contains triangle cycles with k = 3 (for example, tetrahedrane derivatives [9-10] and Ladenburg's benzene [11]). The values of k = 4÷8 are prevalent, because it provides more energetically favorable valence angles. Larger cycles with k > 8 often tend to split into two smaller ones via forming of additional carbon-carbon bond between the opposite atoms.

The square cycles (k = 4) are quite strain. The angle between C-C bonds of about 90º is far from the typical values of 109.5º (as in diamond) or 120º (as in graphite). Nevertheless, a number of structures with the square cycles were found to be stable, for example, cubane [12-13] and its derivatives [14-16], prismanes [17] and hypercubane [18]. Moreover, some "non-classical" fullerenes with square cycles on its surfaces are even more stable than the "classical" ones [19-22]. Four-membered rings are also contained in many recently proposed carbon structures [23-24].

[1] Corresponding author
E-mail: kpkatin@yandex.ru

Boron nitrides form the other promising class of new materials. Both boron and nitrogen atoms are the nearest neighbors to carbon in the Mendeleev's table. For this reason, many carbon architectures have boron nitride analogues, consisted of alternated boron and nitrogen atoms instead of carbon ones. So, boron nitride fullerenes [25], nanotubes [26,27] and other structures [28-30] are actively investigated. Construction of boron nitrides based on already known carbon cages was an efficient way of searching new BN materials. Similar to carbon compounds, some boron nitrides also include four-membered B-N-B-N cycles [31-32].

Most computational studies of novel boron nitrides are based on density functional theory. The commonly used exchange-correlation functionals are B3LYP [33-34] and PBE [35], because they provide high accuracy for many systems [36-37], including boron nitride species [38]. Nevertheless, these functionals were not tested on high-strained boron nitrides with square cycles. For this reason, their application to such untypical systems remains questionable.

In this study, we perform a benchmark study of 24 exchange-correlation functionals on a set of small boron nitride clusters including those with the square cycles. The results, obtained with the density functional theory, were compared with the more accurate data derived from coupled clusters calculations [39-41].

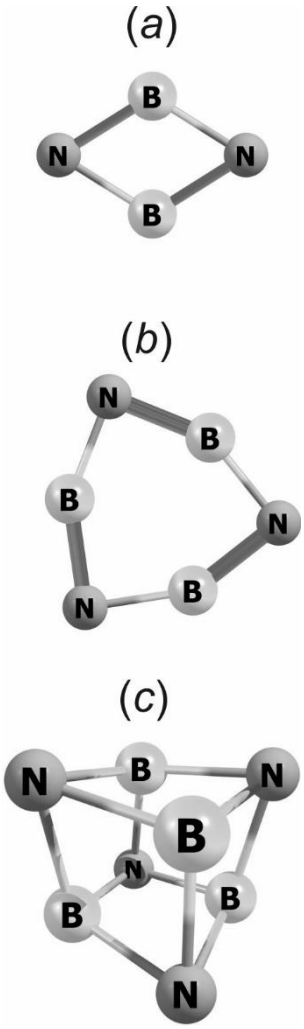

Figure 1. Structures of small boron nitride clusters B_2N_2 (a), B_3N_3 (b) and B_4N_4 (c).

2. Materials and Methods

To test different density functional methods, we chose three boron nitride clusters C_2N_2, C_3N_3 and C_4N_4 with alternated boron and nitrogen atoms. Their structures are presented at Figure 1. Geometries of all three systems were optimized within the density functional and coupled clusters methods until the forces acting on atoms become smaller than 10^{-4} Ha/Bohr. No symmetry constrains were introduces. To confirm that the obtained geometries are true minima on the potential energy hypersurface, we calculate the Hessian matrix at the same level of theory. All considered structures have not any imaginary frequencies and therefore correspond to metastable states.

The values of l_{BN}, a_{BNB} and a_{NBN} for each cluster are calculated as the arithmetic means of all B-N bonds lengths, B-N-B and N-B-N angles, respectively (note, that all averaged numbers, corresponding to the same molecule, are almost the same due to the symmetries of the considered systems). The chemical potentials μ are evaluated according to the Koopmans theorem [42] as $\mu = (E_{HOMO} + E_{LUMO})/2$, where E_{HOMO} and E_{LUMO} are the energies of the highest occupied molecular orbital (HOMO) and the lowest unoccupied molecular orbital (LUMO), respectively.

In our density functional calculations, we compare the follow exchange-correlation functionals: B3LYP [33-34], B3LYPV1R [43], B3P86V5 [34], B3PW91 [34], B97 [44], B97-2 [45], B97-3 [46], B97-K [47], CAMB3LYP [48],

LYP [49], M11 [50], OP [49], PBE0 [51], PW91C [52], VWN [53], VWN1RPA [54], wB97 [55-56], wB97X [55-56], wB97X-D [55-56], X3LYP [57], BMK [47], dLDF [58], M05 [59], M06 [60]. The results are compared with the data obtained with the coupled clusters CCSD(T) method [61]. For all calculations, we use the same 6-311G(2d,2p) basic set [62]. Since we restrict our study by the only singlet configurations, the restricted Hartree-Fock method of self-consistent field calculation is applied. All calculations are performed with the GAMESS software [63].

As a measure of difference between geometries, obtained with coupling clusters and density functional methods, we use the value

$$\varepsilon_g = \frac{1}{N}\sum |x_{CC} - x_{DFT}|/x_{CC}. \quad (1)$$

Here x is one of the geometric parameters (l_{BN}, a_{BNB} or a_{NBN}), N = 9 is the number of terms, summation is performed over all parameters of all considered clusters, indices "CC" and "DFT" correspond to coupled clusters and density functional methods, respectively. A very similar value εe is used as a measure of difference of electronic properties. In this case, x is the chemical potential μ or it means partial Mulliken q_M or Lowdin q_L charge of boron atoms.

3. Results and Discussion

In all three considered boron nitride structures, optimized with the coupled clusters method, all obtained B-N bonds lengths are the same. They are equal to 1.409, 1.363 and 1.511 Å for B_2N_2, B_3N_3 and B_4N_4 clusters, respectively. The value for cubane B_4N_4 (see Figure 1c) slightly differs from the earlier reported coupled clusters results (1.492 [64] and 1.505 Å [65]). However, the authors of Ref. [64] performed only single point calculation of pre-optimized structure, whereas the authors of Ref. [65] applied the CCSD method with symmetry constrains. So, reported here CCSD(T) results are obtained with the higher level of theory and should be regarded as the most accurate.

In Table 1, we present all geometry parameters of considered boron nitride clusters. We can see that the bonds lengths and valence angles, obtained with the density functional methods, differ from the coupled clusters data by ~0.01 Å and ~1º, respectively. The calculated electronic parameters are listed at Table 2. Chemical potentials are compared well with the each other, whereas partial charges demonstrate huge dispersions.

Table 1. Geometric parameters l_{BN} (Å), a_{BNB} and a_{NBN} (degree) of clusters B_2N_2, B_3N_3 and B_4N_4, obtained with the CCSD(T) method. The differences between l_{BN}, a_{BNB} and a_{NBN} values, calculated with the CCSD(T) and DFT approaches, are also listed.

Method	B_2N_2			B_3N_3			B_4N_4		
	l_{BN}	a_{BNB}	a_{NBN}	l_{BN}	a_{BNB}	a_{NBN}	l_{BN}	a_{BNB}	a_{NBN}
CCSD(T)	**1.409**	**63.81**	**116.19**	**1.363**	**88.32**	**151.68**	**1.511**	**75.37**	**102.91**
B3LYP	-0.017	0.46	-0.46	-0.010	0.87	-0.87	-0.010	0.18	-0.14
B3LYPV1R	-0.017	0.46	-0.46	-0.010	0.88	-0.88	-0.010	0.18	-0.14
B3P86V5	-0.015	0.31	-0.31	-0.008	0.03	-0.04	-0.011	-0.13	0.10
B3PW91	-0.016	0.27	-0.27	-0.009	-0.22	0.23	-0.012	-0.26	0.20
B97	-0.012	0.56	-0.57	-0.005	-0.09	0.09	-0.006	0.19	-0.15
B97-2	-0.014	0.15	-0.15	-0.008	-0.36	0.36	-0.012	-0.60	0.46
B97-3	-0.017	0.49	-0.49	-0.010	0.03	-0.03	-0.013	0.01	-0.01
B97-K	-0.013	0.68	-0.68	-0.007	0.37	-0.37	-0.007	0.00	0.00
CAMB3LYP	-0.025	0.71	-0.71	-0.016	1.50	-1.50	-0.018	0.18	-0.14
LYP	-0.045	1.42	-1.42	-0.036	2.87	-2.87	-0.042	0.15	-0.12
M11	-0.019	0.84	-0.84	-0.010	0.86	-0.86	-0.011	-0.78	0.59
OP	-0.042	1.36	-1.36	-0.033	2.58	-2.58	-0.039	0.00	0.00
PBE0	-0.017	0.25	-0.25	-0.228	-0.37	0.37	-0.014	-0.40	0.31
PW91C	-0.044	1.23	-1.23	-0.035	1.94	-1.93	-0.043	-0.25	0.19
VWN	-0.045	1.43	-1.43	-0.036	2.87	-2.86	-0.018	0.19	-0.14
VWN1RPA	-0.047	1.44	-1.44	-0.037	2.80	-2.86	-0.043	0.06	-0.04
wB97	-0.017	0.42	-0.42	-0.008	-0.30	0.30	-0.013	-1.13	0.86
wB97X	-0.020	0.59	-0.59	-0.011	0.27	-0.27	-0.015	-0.53	0.41
wB97X-D	-0.020	0.78	-0.78	-0.011	0.19	-0.18	-0.015	-0.02	0.01

Table 1 continued

X3LYP	-0.018	0.50	-0.50	-0.011	0.98	-0.98	-0.011	0.19	-0.15
BMK	-0.026	1.32	-1.32	-0.015	-0.97	0.97	-0.019	0.15	-0.11
dLDF	-0.014	0.38	-0.38	-0.009	1.62	-1.62	-0.006	-0.95	0.72
M05	-0.017	-0.13	0.13	-0.007	-3.23	3.23	-0.014	-1.89	1.42
M06	-0.022	0.19	-0.19	-0.015	-0.24	0.24	-0.018	-0.67	0.51

Table 2. Chemical potentials μ (eV), mean Mulliken q_M or Lowdin q_L charges of boron atoms (|e|, where e is the elementary charge) of clusters B_2N_2, B_3N_3 and B_4N_4, obtained with the CCSD(T) method. The differences between the values, calculated with the CCSD(T) and DFT approaches, are also listed.

Method	B_2N_2			B_3N_3			B_4N_4		
	μ	q_M	q_L	μ	q_M	q_L	μ	q_M	q_L
CCSD(T)	**-5.73**	**-0.437**	**0.040**	**-5.60**	**-0.275**	**0.128**	**-6.37**	**-0.513**	**0.146**
B3LYP	-0.20	0.144	0.083	-0.21	0.166	0.066	-0.04	0.178	0.081
B3LYPV1R	-0.29	0.143	0.083	-0.30	0.165	0.066	-0.12	0.177	0.081
B3P86V5	-0.39	0.128	0.082	-0.43	0.142	0.069	-0.25	0.157	0.087
B3PW91	-0.29	0.129	0.081	-0.33	0.140	0.069	-0.16	0.155	0.087
B97	-0.18	0.125	0.072	-0.22	0.150	0.064	-0.04	0.158	0.075
B97-2	-0.18	0.139	0.074	-0.19	0.134	0.061	-0.04	0.169	0.083
B97-3	-0.21	0.116	0.070	-0.26	0.141	0.061	-0.10	0.138	0.075
B97-K	-0.17	0.104	0.061	-0.21	0.138	0.057	-0.10	0.135	0.067
CAMB3LYP	-0.39	0.147	0.084	-0.41	0.174	0.066	-0.24	0.185	0.084
LYP	-0.74	0.018	0.024	-0.75	0.032	0.013	-0.73	0.053	0.038
M11	-0.45	-0.014	0.075	-0.56	-0.055	0.059	-0.40	0.043	0.085
OP	-0.62	0.001	0.016	-0.63	0.001	0.006	-0.62	0.027	0.031
PBE0	-0.28	0.141	0.081	-0.34	0.152	0.072	-0.17	0.189	0.092
PW91C	-0.82	0.003	0.021	-0.87	-0.002	0.015	-0.85	0.025	0.045
VWN	-1.13	-0.006	0.010	-1.12	-0.003	-0.004	-1.12	0.021	0.022
VWN1RPA	-1.60	-0.009	0.009	-1.59	-0.004	-0.004	-1.59	0.020	0.022
wB97	-0.28	0.134	0.069	-0.37	0.145	0.059	-0.21	0.165	0.082
wB97X	-0.29	0.130	0.070	-0.36	0.148	0.060	-0.24	0.184	0.088
wB97X-D	-0.26	0.103	0.066	-0.32	0.130	0.059	-0.14	0.118	0.073
X3LYP	-0.25	0.146	0.084	-0.27	0.170	0.067	-0.10	0.845	0.082
BMK	-0.30	0.024	0.054	-0.39	0.135	0.069	-0.20	0.094	0.071
dLDF	-0.66	0.081	0.033	-0.66	0.069	0.008	-0.62	0.099	0.033
M05	-0.13	0.120	0.066	-0.28	0.171	0.066	-0.04	0.124	0.086
M06	-0.27	0.074	0.068	-0.33	0.095	0.053	-0.13	0.038	0.074

The mean geometry and electronic errors (ε_g and ε_e), calculated with different exchange-corrected functionals using formula (1), are collected at Table 3. We conclude that B3P86V5 and B97 functionals reproduce well the geometries, whereas the OP and VWN provide the best matches of electronic properties. OP and VWN functionals also provide the minimal values of $\varepsilon_g + \varepsilon_e$. Using of popular B3LYP and PBE0 functionals results in higher errors εg and εe.

Table 3. The values of mean errors ε_g and ε_e for different exchange-corrected functionals (see formula (1) for details). The sums of two errors are also presented.

functional	ε_g	ε_e	$\varepsilon_g + \varepsilon_e$
B3LYP	0.0063	0.5003	0.5066
B3LYPV1R	0.0063	0.5045	0.5108
B3P86V5	**0.0038**	0.4981	0.5019
B3PW91	0.0047	0.4892	0.4939
B97	**0.0039**	0.4476	0.4515
B97-2	0.0051	0.4558	0.4609
B97-3	0.0045	0.4319	0.4364
B97-K	0.0047	0.3905	0.3952
CAMB3LYP	0.0099	0.5224	0.5323
LYP	0.0195	0.1777	0.1972
M11	0.0089	0.3862	0.3951
OP	0.0177	**0.1151**	**0.1328**
PBE0	0.0233	0.5108	0.5341
PW91C	0.0172	0.1605	0.1777
VWN	0.0178	**0.1190**	**0.1368**
VWN1RPA	0.0196	0.1438	0.1634
wB97	0.0073	0.4501	0.4574
wB97X	0.0069	0.4631	0.4700
wB97X-D	0.0061	0.4082	0.4143
X3LYP	0.0069	0.6547	0.6616
BMK	0.0105	0.3620	0.3725
dLDF	0.0087	0.2304	0.2391
M05	0.0140	0.4413	0.4553
M06	0.0068	0.3708	0.3776

4. Conclusion

In the study presented, we perform a comparable analysis of density functional approaches applied to the small boron nitride clusters. The data obtained provide a reasonable choice of the most suitable exchange-corrected DFT-functional for strained BN-systems numerical simulation. We consider that the reported results stimulate further density functional studies not only of pristine boron nitrides, but also of their strained analogues such as prismanes, non-classical fullerenes, and silicic cages both in molecular and crystalline forms.

References

[1] M. Monthioux, Filling single-wall carbon nanotubes, Carbon 40 (2002) 1809–1823.

[2] W. Krätschmer, D. R. Huffman, Fullerites: New forms of crystalline carbon, Carbon 30 (1992) 1143–1147.

[3] E. A. Belenkov, V. A. Greshnyakov, New structural modifications of diamond: LA9, LA10, and CA12, Journal of Experimental and Theoretical Physics 119 (2014) 101–106.

[4] V. A. Greshnyakov, E. A. Belenkov, Structures of diamond-like phases, Journal of Experimental and Theoretical Physics 113 (2011) 86–95.

[5] Y. A. Kvashnina, A. G. Kvashnin, P. B. Sorokin, Investigation of new superhard carbon allotropes with promising electronic properties, Journal of Applied Physics 114 (2013) 183708.

[6] Yu. A. Kvashnina, A. G. Kvashnin, M. Yu. Popov, B. A. Kulnitskiy, I. A. Perezhogin, E. V. Tyukalova, L. A. Chernozatonskii, P. B. Sorokin, V. D. Blank, Toward the Ultra-incompressible Carbon Materials. Computational Simulation and Experimental Observation, Journal of Physical Chemistry Letters 6 (2015) 2147–2152.

[7] R. A. Brazhe, A. A. Karenin, A. I. Kochaev, R. M. Meftakhutdinov, Elastic characteristics of 2D carbon supracrystals as compared to graphene, Physics of the Solid State 53 (2011) 1481–1483.

[8] R. A. Brazhe, A. I. Kochaev, V. S. Nefedov, Young's modulus and the Poisson's ratio of planar and nanotubular supracrystalline structures, Physics of the Solid State 54 (2012) 1430–1432.

[9] G. Maier, S. Pfriem, U. Schäfer, R. Matusch, Tetra-tert-butyltetrahedrane, Angewandte Chemie International Edition 17 (1978) 520–521.

[10] G. Maier, D. Born, Tri-tert-butyl(trimethylsilyl)tricyclo[1.1.0.02, 4]-butane–a Second Tetrahedrane Derivative, Angewandte Chemie International Edition 28 (1989) 1050–1052.

[11] T. J. Katz, N. Acton, Synthesis of prismane, Journal of the American Chemical Society 95 (1973) 2738–2739.

[12] P. E. Eaton, T. W. Cole, Cubane, Journal of the American Chemical Society 86 (1964) 3157–3158.

[13] P. E. Eaton, Cubanes: Starting Materials for the Chemistry of the 1990s and the New Century, Angewandte Chemie International Edition 31 (1992) 1421–1436.

[14] K. A. Lukin, J. Li, P. E. Eaton, N. Kanomata, J. Hain, E. Punzalan, R. Gilardi, Synthesis and chemistry of 1,3,5,7-tetranitrocubane including measurement of its acidity,

formation of o-nitro anions, and the first preparations of pentanitrocubane and hexanitrocubane, Journal of the American Chemical Society 119 (1997) 9591–9602.

[15] M. X. Zhang, P. E. Eaton, R. Gilardi, Hepta- and octanitrocubanes, Angewandte Chemie International Edition39 (2000) 401–404.

[16] P. E. Eaton, M. X. Zhang, R. Gilardi, N. Gelber, S. Iyer, R. Surapaneni, Octanitrocubane: A new nitrocarbon, Propellants, Explosives, Pyrotechnics 27 (2002) 1–6.

[17] P. E. Eaton, Y. S. Or, S. J. Branca, Pentaprismane, Journal of the American Chemical Society 103 (1981) 2134–2136.

[18] F. Pichierri, Hypercubane: DFT-based prediction of an Oh-symmetric double-shell hydrocarbon, Chemical Physics Letters 612 (2014) 198–202.

[19] C. Killblane, Y. Gao, N. Shao, X. C. Zeng, Search for Lowest-Energy Nonclassical Fullerenes III: C22, Journal of Physical Chemistry A 113 (2009) 8839–8844.

[20] W. An, N. Shao, S. Bulusu, X. C. Zeng, Ab initio calculation of carbon clusters. II. Relative stabilities of fullerene and nonfullerene C24, Journal of Chemical Physics 128 (2008) 084301.

[21] J. An, L. H. Gan, J. Q. Zhao, R. Li, A global search for the lowest energy isomer of C26, Journal of Chemical Physics 132 (2010) 154304.

[22] W. W. Wang, J. S. Dang, X. Zhao, Impact of tetragonal rings on the stability of small fullerenes encapsulated with noble gas: A density functional theory survey, Chemical Physics Letters 536 (2012) 77–81.

[23] Y. A. Kvashnina, D. G. Kvashnin, A. G. Kvashnin, P. B. Sorokin, New allotropic forms of carbon based on C60 and C20 fullerenes with specific mechanical characteristics, JETP Letters 105 (2017) 419–425.

[24] D. S. Lisovenko, J. A. Baimova, L. K. Rysaeva, V. A. Gorodtsov, A. I. Rudskoy, S. V. Dmitriev, Equilibrium diamond-like carbon nanostructures with cubic anisotropy: Elastic properties, Physica Status Solidi B 253 (2016) 1295–1302.

[25] X. Xia, D. A. Jelski, J. R. Bowser, T. F. George, MNDO Study of Boron-Nitrogen Analogs of Buckminsterfullerene, Journal of the American Chemical Society 114 (1992) 6493–6496.

[26] E. J. Hamilton, S. E. Dolan, C. M. Mann, H. O. Colijn, C. a McDonald, S. G. Shore, Preparation of amorphous boron nitride and its conversion to a turbostratic, tubular form, Science 260 (1993) 659–661.

[27] A. Loiseau, F. Willaime, N. Demoncy, G. Hug, H. Pascard, Boron Nitride Nanotubes with Reduced Numbers of Layers Synthesized by Arc Discharge, Physical Review Letters 76 (1996) 4737–4740.

[28] L. Bourgeois, Y. Bando, S. Shinozaki, K. Kurashima, T. Sato, Boron nitride cones: structure determination by transmission electron microscopy, Acta Crystallographica A 55 (1999) 168–177.

[29] L. Bourgeois, Y. Bando, W. Han, T. Sato, Structure of boron nitride nanoscale cones: Ordered stacking of 240° and 300° disclinations, Physical Review B 61 (2000) 7686–7691.

[30] K. Terauchi, M., Tanaka, M., Suzuki, K., Ogino, A., Kimura, Nanotubes, Production of zigzag-type BN Annealing, and BN cones by thermal, Chemical Physics Letters 324 (2000) 359–364.

[31] M. T. Baei, H. Mohammadian, S. Hashemian, B12N12 nanocage as a potential adsorbent for the removal of aniline from environmental systems, Bulgarian Chemical Communications 46 (2014) 735–742.

[32] M. D. Esrafili, S. Chashmniam, V. Alizadeh, A DFT Study of Hydrogen Adsorption on Ln@B16N16 Fullerene-Like Nanocage (Ln: La, Gd and Lu), Fullerenes, Nanotubes and Carbon Nanostructures 22 (2014) 928–937.

[33] C. Lee, W. Yang, R. G. Parr, Development of the Colle-Salvetti correlation-energy formula into a functional of the electron density, Physical Review B 37 (1988) 785–789.

[34] A. D. Becke, Density-functional thermochemistry. III. The role of exact exchange, Journal of Chemical Physics 98 (1993) 5648–5652.

[35] J. P. Perdew, K. Burke, M. Ernzerhof, Generalized Gradient Approximation Made

Simple, Physical Review Letters 77 (1996) 3865–3868.

[36] J. G. Brandenburg, T. Maas, S. Grimme, Benchmarking DFT and semiempirical methods on structures and lattice energies for ten ice polymorphs, Journal of Chemical Physics 142 (2015) 124104.

[37] É. Brémond, M. Savarese, N. Q. Su, Á. J. Pérez-Jiménez, X. Xu, J. C. Sancho-García, C. Adamo, Benchmarking Density Functionals on Structural Parameters of Small-/Medium-Sized Organic Molecules, Journal of Chemical Theory and Computation 12 (2016) 459–465.

[38] D. Karakas, Theoretical investigation on electrophilicity indexes and proton affinities of some boron-nitrogen open-chain species, Turkish Computational and Theoretical Chemistry 1 (2017) 1–10.

[39] K. Raghavachari, G. W. Trucks, J. A. Pople, M. Head-Gordon, Reprint of: A fifth-order perturbation comparison of electron correlation theories, Chemical Physics Letters 589 (2013) 37–40.

[40] H. J. Monkhorst, Calculation of properties with the coupled-cluster method, International Journal of Quantum Chemistry 12 (1977) 421–432.

[41] P. Piecuch, S. A. Kucharski, K. Kowalski, M. Musiał, Efficient computer implementation of the renormalized coupled-cluster methods: The R-CCSD[T], R-CCSD(T), CR-CCSD[T], and CR-CCSD(T) approaches, Computer Physics Communications 149 (2002) 71–96.

[42] T. Koopmans, Über die Zuordnung von Wellenfunktionen und Eigenwerten zu den Einzelnen Elektronen Eines Atoms, Physica 1 (1934) 104–113.

[43] P. J. Stephens, F. J. Devlin, C. F. Chabalowski, M. J. Frisch, Ab initio calculation of vibrational absorption and circular dichroism spectra using density functional force fields, Journal of Chemical Physics 98 (1994) 11623–11627.

[44] A. D. Becke, Density-functional thermochemistry. V. Systematic optimization of exchange-correlation functionals, Journal of Chemical Physics 107 (1997) 8554-8560.

[45] P. J. Wilson, T. J. Bradley, D. J. Tozer, Hybrid exchange-correlation functional determined from thermochemical data and ab initio potentials, Journal of Chemical Physics 115 (2001) 9233-9242.

[46] T. W. Keal, D. J. Tozer, Semiempirical hybrid functional with improved performance in an extensive chemical assessment, Journal of Chemical Physics 123 (2005) 121103.

[47] A. D. Boese, J. M. L. Martin, Development of density functionals for thermochemical kinetics, Journal of Chemical Physics 121 (2004) 3405-3416.

[48] T. Yanai, D. P. Tew, N. C. Handy, A new hybrid exchange–correlation functional using the Coulomb-attenuating method (CAM-B3LYP), Chemical Physics Letters 393 (2004) 51–57.

[49] T. Tsuneda, K. Hirao, A new spin-polarized Colle-Salvetti-type correlation energy functional, Chemical Physics Letters 268 (1997) 510-520.

[50] R. Peverati, D. G. Truhlar, Improving the accuracy of hybrid meta-GGA density functionals by range separation, Journal of Physical Chemistry Letters 2 (2011) 2810-2817.

[51] C. Adamo, V. Barone, Toward reliable density functional methods without adjustable parameters: The PBE0 model, Journal of Chemical Physics 110 (1999) 6158-6170.

[52] J. P. Perdew, Y. Wang, Accurate and simple analytic representation of the electron gas correlation energy, Physical Review B 45 (1992) 13244–13249.

[53] S. H. Vosko, L. Wilk, M. Nusair, Accurate spin-dependent electron liquid correlation energies for local spin density calculations: a critical analysis, Canadian Journal of Physics 58 (1980) 1200-1211.

[54] P. Salek, A. Hesselmann, A self-contained and portable density functional theory library for use in Ab Initio quantum chemistry programs, Journal of Computational Chemistry 28 (2007) 2569-2575.

[55] J. D. Chai, M. Head-Gordon, Systematic optimization of long-range corrected hybrid density functionals, Journal of Chemical Physics 128 (2008) 084106.

[56] J. D. Chai, M. Head-Gordon, Long-range corrected hybrid density functionals with damped atom–atom dispersion corrections,

Physical Chemistry Chemical Physics 10 (2008) 6615-6620.

[57] X. Xu, Q. Zhang, R. P. Muller, W. A. Goddard, An extended hybrid density functional (X3LYP) with improved descriptions of nonbond interactions and thermodynamic properties of molecular systems, Journal of Chemical Physics 122 (2005) 014105.

[58] K. Pernal, R. Podeszwa, K. Patkowski, K. Szalewicz, Dispersionless Density Functional Theory, Physical Review Letters 103 (2009) 263201.

[59] Y. Zhao, N. E. Schultz, D. G. Truhlar, Exchange-correlation functional with broad accuracy for metallic and nonmetallic compounds, kinetics, and noncovalent interactions, Journal of Chemical Physics 123 (2005) 161103.

[60] Y. Zhao, D.G. Truhlar, The M06 suite of density functionals for main group thermochemistry, thermochemical kinetics, noncovalent interactions, excited states, and transition elements: two new functionals and systematic testing of four M06-class functionals and 12 other functionals, Theoretical Chemistry Accounts 120 (2007) 215-241.

[61] T. Helgaker, P. Jorgensen, J. Olsen. Molecular Electronic-Structure Theory. Wiley: New York, 2000, 793-796.

[62] R. Krishnan, J. S. Binkley, R. Seeger, J. A. Pople, Self-consistent molecular orbital methods. XX. A basis set for correlated wave functions, Journal of Chemical Physics 72 (1980) 650–654.

[63] M. W. Schmidt, K. K. Baldridge, J. A. Boatz, S. T. Elbert, M. S. Gordon, J. H. Jensen, S. Koseki, N. Matsunaga, K. A. Nguyen, S. Su, T. L. Windus, M. Dupuis, J. A. Montgomery Jr, General atomic and molecular electronic structure system, Journal of Computational Chemistry 14 (1993) 1347–1363.

[64] F. Jensen, The stability of cage and ring isomers for carbon and boron nitride clusters, Chemical Physics Letters 209 (1993) 417–422.

[65] M. R. Manaa, A comparative study of cubic B4N4 and C8, Journal of Molecular Structure: THEOCHEM 549 (2001) 23–26.

Turkish Computational and Theoretical Chemistry

Turkish Comp Theo Chem (TC&TC)

Volume(Issue): 1(2) – Year: 2017 – Pages: 35-44

ISSN: 2587-1722 / e-ISSN: 2602-3237

Received: 27.10.2017 **Accepted:** 07.11.2017 *Research Article*

Determination of Inhibition Mechanism of Mono-Azo Naphthylamine Dyes: A Computational Corrosion Study

Nihat KARAKUŞ[1]

Department of Chemistry, Faculty of Science, Cumhuriyet University, 58140 Sivas, Turkey

Abstract: Some mono azo naphthylamine dyes are optimized by using HF, B3LYP and M062X with 6-31G(d) level in gas phase. The best level is found as HF/6-31G(d) level in gas phase. A well agreement between experimental results and calculated results is found. Contour diagram of frontier molecular orbitals, MEP maps, MEP contours, NBO analyses and Fukui functions are calculated and examined in detail to foresee the corrosion protection mechanism. Regression and matrix analyses are used to derive the new theoretical formula. Experimental and theoretical formula are compared with each other and well agreement is calculated among of them.

Keywords: *Naphthylamine, Ab-initio, DFT, Molecular Modelling, Quantum Chemical Descriptors.*

Graphical Abstract

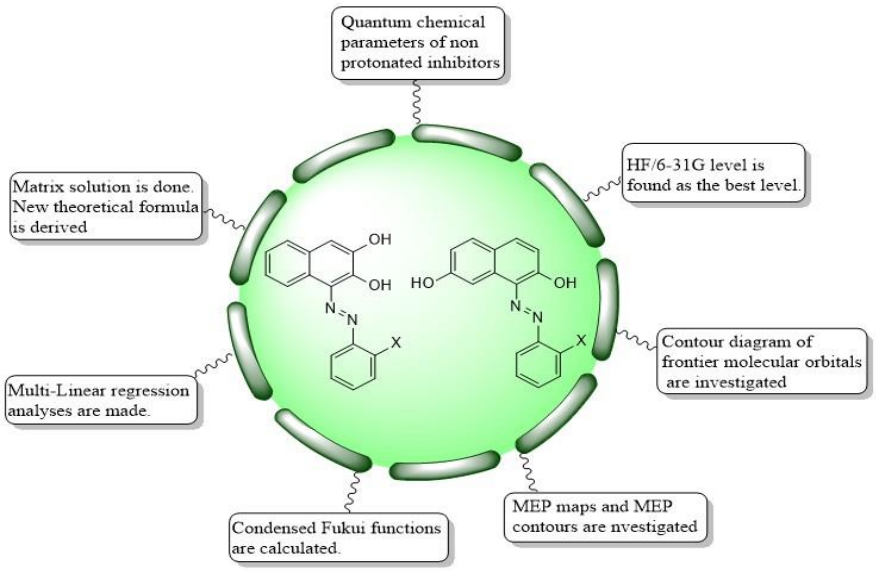

- Investigations of anti-corrosive properties are performed by using HF, B3LYP and M062X methods.
- HF/6-31G(d) is found as the best calculation level and it is taken into consideration in other calculations
- Corrosion protection mechanism is predicted by using MEP maps, MEP contours, Fukui functions and contour diagram of FMOs.
- New theoretical formula is derived by multi-linear regression analyses and matrix solution.

[1] Corresponding Author

e-mail: nkarakus@cumhuriyet.edu.tr

1. Introduction

Corrosion means the gradual destruction of materials by chemical and/or electrochemical reaction with their environment [1-3]. Controlling and stopping corrosion is so important for industries. Corrosion affects people and industries and their environment. Investigations of anti-corrosive properties, therefore, are important and will continue throughout human life. Large investments are made in this regard and many experiments are carried out. Inhibitors are used in corrosion prevention and their efficiency ranking can be learned by experimental or computational methods [4-12]. Computational research has many advantages and gives important results to experimental works. There are a lot of computational research over corrosion in literature.

Selected mono azo naphthylamine dyes have been synthesized by Mabrouk et al. in 2011 and their corrosion inhibition efficiencies have been investigated toward aluminum in 2M HCl solutions [13]. In their study, weight loss, thermometry and galvanostatic polarization techniques have been used. In this study, mentioned inhibitors are investigated via computational methods. HF, B3LYP and M062X methods are used with 6-31G(d) basis set in calculations. Fully optimizations are carried out and some quantum chemical descriptors are determined. These descriptors are energy of the highest occupied molecular orbital (EHOMO), energy of the lowest unoccupied molecular orbital (ELUMO), energy gap among frontier molecular orbitals (EGap), chemical hardness (η), chemical softness (σ), absolute electronegativity (χ), electrophilicity index (ω) and nucleophilicity index (N). These descriptors are often used in foreseeing the inhibition efficiency ranking on inhibitors or reactivity ranking of chemicals. These parameters are calculated from results of optimized structures in each level. Then, experimental inhibition efficiency ranking is compared with calculated results. In this way, the best calculation level is determined. This level is used in the prediction of corrosion mechanism and in the derivation of theoretical formula. In the determination of corrosion mechanism, molecular electrostatic potential (MEP) map, MEP contour, contour diagram of HOMO and LUMO, natural bond orbital (NBO) analyses and Fukui functions are used. Additionally, the most compatible descriptors are determined by regression analyses.

2. Method

Computational investigations of mono azo naphthylamine dyes were performed via Gaussian package program which are Gauss View 5.0.8 [14], Gaussian 09 IA32W-G09RevA.02 [15] and Gaussian 09 AML64-G09RevD.01 [16]. Pre-calculations were done by personal computers and full calculations were carried out via Linux server in TÜBİTAK TR-Grid from TURKEY. Additionally, ChemBioDraw Ultra Version (13.0.0.3015) program was used in preparation of some figures [17]. Hartree-Fock (HF) [18] and hybrid density functional theory (DFT) functionals, B3LYP [19] and M062X [20] methods, was used in calculation with 6-31G(d) basis set. No imaginary frequency was observed in results of calculation. Mentioned quantum chemical descriptors are via Eq. (1) – (9) [21–28]. In calculation of these parameters, Koopmans theorem was taken into account [29]. Fukui functions for nucleophilic attack (f_k^+), electrophilic attack (f_k^-) and radicalic attack (f_k^0) are calculated [30]. For a system of N electron, fully optimizations are performed at the same level of theory for corresponding systems of (N + 1) and (N – 1) electron. The natural population analysis yields to $P_k(N-1)$, $P_k(N)$ and $P_k(N+1)$; the population for all k atoms.

$$I = -E_{HOMO} \tag{1}$$

$$A = -E_{LUMO} \tag{2}$$

$$E_{GAP} = E_{LUMO} - E_{HOMO} \tag{3}$$

$$\eta = \frac{I - A}{2} = \frac{E_{LUMO} - E_{HOMO}}{2} \tag{4}$$

$$\sigma = \frac{1}{\eta} \tag{5}$$

$$\chi = \frac{|I + A|}{2} = \frac{|-E_{HOMO} - E_{LUMO}|}{2} \tag{6}$$

$$CP = -\chi \tag{7}$$

$$\omega = \frac{CP^2}{2\eta} \quad (8)$$

$$N = \frac{1}{\omega} \quad (9)$$

$$f_k^+ = P_k(N+1) - P_k(N) \quad (10)$$

$$f_k^- = P_k(N1) - P_k(N-1) \quad (11)$$

$$f_k^0 = \frac{P_k(N+1) - P_k(N-1)}{2} \quad (12)$$

3. Results and discussion

3.1. Optimized Geometry

Investigated inhibitors are optimized at HF/6-31G(d), B3LYP/6-31G(d) and M062X/6-31G(d) levels in gas phase. Schematic and optimized structures of studied inhibitors are given in Fig. 1. Calculated quantum chemical descriptors are given in Table 1 at HF/6-31G(d), B3LYP/6-31G(d) and M062X/6-31G(d) levels.

The energy of HOMO is significant descriptors in explanation of anti-corrosion properties of related molecules. The high value of its means that inhibitor may easily coordinate to metal surface by giving electrons. Hence, inhibition efficiency of inhibitors increases with increasing of E_{HOMO}. The energy value of LUMO is a descriptor which is used by researcher in determination of inhibition efficiency ranking. Tendency of coordinating increases with the lower energy value of LUMO. Another descriptor is energy gap between frontier molecular orbitals. Electron mobility is important subject in explanation of anti-corrosive properties of inhibitors. Electron mobility increases with decreasing of energy gap. Hence, anti-corrosive properties of inhibitors increase with decreasing of EGAP. In addition to these parameters, chemical hardness and chemical softness is considerable descriptor. Since, metallic bulks are known as chemical soft structure. They prefer to interact with soft molecule. Thence, the increasing of chemical softness increases the inhibition efficiency of molecules. Another parameter is electronegativity. Decreasing of electronegativity implies the increasing of anti-corrosion properties. The last parameters are electrophilicity and nucleophilicity indexes. Increasing of nucleophilicity index or decreasing of electrophilicity index increases the coordination tendency of inhibitor against metallic surface. Therefore, it is expected that inhibition efficiency increases with increasing of nucleophilicity index. According to above explanations, inhibition efficiency ranking for each descriptor should be as follow.

According to E_{HOMO} **(IV)** > **(III)** > **(II)** > **(I)** (HF)
(IV) > **(III)** > **(II)** > **(I)** (B3LYP)
(IV) > **(III)** > **(II)** > **(I)** (M062X)

According to E_{LUMO} **(III)** > **(IV)** > **(II)** > **(I)** (HF)
(II) > **(I)** > **(IV)** > **(III)** (B3LYP)
(II) > **(I)** > **(IV)** > **(III)** (M062X)

According to E_{GAP} **(IV)** > **(III)** > **(II)** > **(I)** (HF)
(II) > **(I)** > **(IV)** > **(III)** (B3LYP)
(II) > **(I)** > **(IV)** > **(III)** (M062X)

According to η and σ **(IV)** > **(III)** > **(II)** > **(I)** (HF)
(II) > **(I)** > **(IV)** > **(III)** (B3LYP)
(II) > **(I)** > **(IV)** > **(III)** (M062X)

According to χ **(IV)** > **(III)** > **(I)** > **(II)** (HF)
(IV) > **(III)** > **(I)** > **(II)** (B3LYP)
(IV) = **(III)** > **(I)** > **(II)** (M062X)

According to ω and N **(IV)** > **(III)** > **(I)** > **(II)** (HF)
(III) > **(IV)** > **(II)** = **(I)** (B3LYP)
(III) > **(IV)** > **(I)** > **(II)** (M062X)

According to above ranking the most compatible ranking is obtained at HF/6-31G(d) level in the gas phase. Hence, this level is taken into account for other calculations. Additionally, calculated general inhibition efficiency ranking is found as follow:

(IV) > **(III)** > **(II)** > **(I)**

Above ranking is in agreement with experimental results. In addition to this result, it is found that electron releasing group (-OCH3) increases the inhibition efficiency of inhibitor while electron donating group (-COOH) decreases the inhibition efficiency of inhibitors.

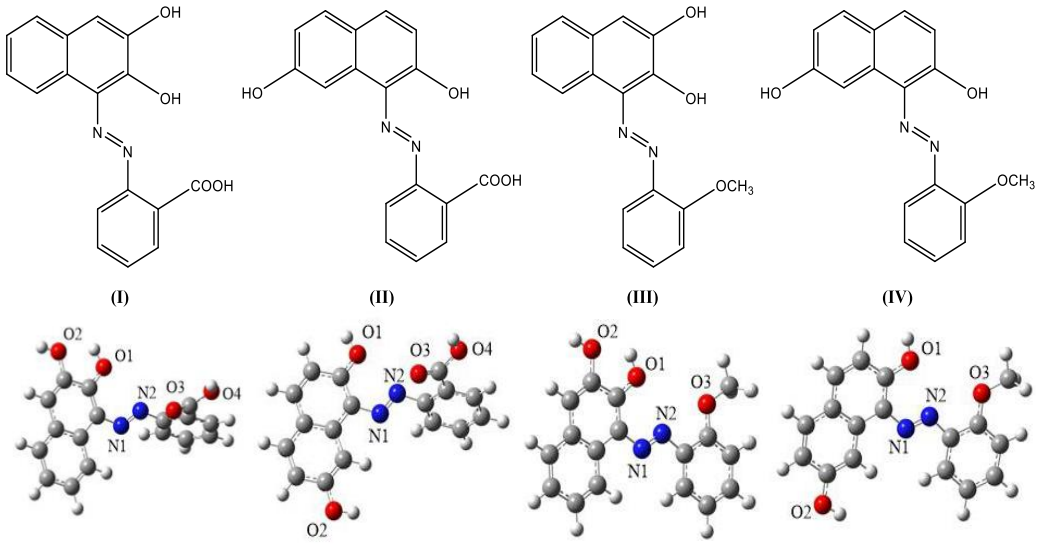

Fig. 1. Schematic and optimized structures of studied mono azo naphthylamine dyes at HF/6-31G(d) level in gas phase.

Table 1. Calculated descriptors for inhibitor **(I) – (IV)** at related levels in gas phase

Inhibitors	E_{HOMO}[1]	E_{LUMO}[1]	E_{GAP}[1]	η[1]	σ[2]	χ[1]	ω[1]	N[2]
HF/6-31G(d)								
Inhibitor **(I)**	-7.614	2.039	9.653	4.827	0.207	2.788	0.805	1.242
Inhibitor **(II)**	-7.602	1.974	9.575	4.788	0.209	2.814	0.827	1.209
Inhibitor **(III)**	-7.325	1.932	9.257	4.629	0.216	2.696	0.785	1.273
Inhibitor **(IV)**	-7.303	1.946	9.249	4.624	0.216	2.679	0.776	1.289
B3LYP/6-31G(d)								
Inhibitor **(I)**	-5.510	-2.218	3.292	1.646	0.607	3.864	4.536	0.220
Inhibitor **(II)**	-5.495	-2.221	3.274	1.637	0.611	3.858	4.545	0.220
Inhibitor **(III)**	-5.223	-1.887	3.337	1.668	0.599	3.555	3.787	0.264
Inhibitor **(IV)**	-5.204	-1.890	3.314	1.657	0.604	3.547	3.797	0.263
M062X/6-31G(d)								
Inhibitor **(I)**	-6.757	-1.282	5.475	2.737	0.365	4.019	2.951	0.339
Inhibitor **(II)**	-6.742	-1.306	5.436	2.718	0.368	4.024	2.978	0.336
Inhibitor **(III)**	-6.518	-0.983	5.535	2.768	0.361	3.750	2.541	0.394
Inhibitor **(IV)**	-6.497	-1.002	5.495	2.747	0.364	3.750	2.559	0.391

[1] in eV, [2] in eV^{-1}

Table 2. Calculated quantum chemical descriptors of inhibitor **(I) – (IV)** at HF/6-31G(d) level in aqua

Inhibitors	E_{HOMO}[1]	E_{LUMO}[1]	E_{GAP}[1]	η[1]	σ[2]	χ[1]	ω[1]	N[2]
Inhibitor **(I)**	-7.913	1.668	9.582	4.791	0.209	3.122	1.018	0.983
Inhibitor **(II)**	-7.763	1.310	9.074	4.537	0.220	3.226	1.147	0.872
Inhibitor **(III)**	-7.662	1.522	9.184	4.592	0.218	3.070	1.026	0.974
Inhibitor **(IV)**	-7.596	1.597	9.193	4.597	0.218	3.000	0.979	1.022

[1] in eV, [2] in eV^{-1}

3.2. Optimization of Inhibitors in Aqua

Investigated compounds are re-optimized at HF/6-31G(d) level in aqua. Related quantum chemical descriptors are re-calculated and given in Table 2.

In terms of quantum chemical descriptors in Table 2, inhibition efficiency ranking of related compounds should be given as follow:

According to E_{HOMO}	**(IV)** > **(III)** > **(II)** > **(I)**
According to E_{LUMO}	**(II)** > **(III)** > **(IV)** > **(I)**
According to E_{GAP}	**(II)** > **(III)** > **(IV)** > **(I)**
According to η and σ	**(II)** > **(III)** > **(IV)** > **(I)**
According to χ	**(IV)** > **(III)** > **(I)** > **(II)**
According to ω and N	**(IV)** > **(I)** > **(III)** > **(II)**

Results in aqua show that these calculations are inadequate in explanation of the anti-corrosion properties. It is determined that computational investigations in water is not appropriate for our studied molecules.

3.3. Prediction of Corrosion Mechanism

The most important stage in corrosion research is determination of corrosion mechanism. If mechanism is determined close to truth, it may be easier to recommend the inhibition efficiency and the anti-corrosive molecules. The first one is contour diagram of frontier molecular orbital and they are represented in Fig. 2.

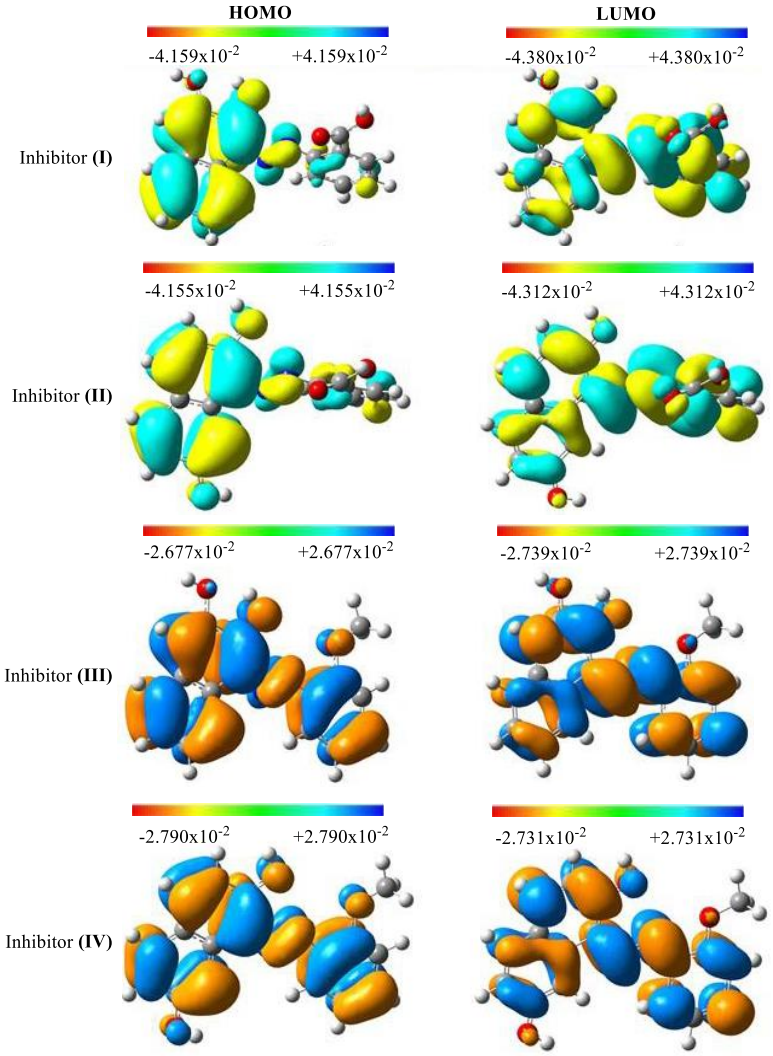

Fig. 2. Contour diagram of frontier molecular orbitals of related compounds at HF/6-31G(d) level in gas phase.

According to Fig. 2, if molecule gives electrons to the metal surface, they belong to HOMO and these electrons are mainly delocalized on the molecule surface. These results showed that π electrons have a significant effect on corrosion protection. Additionally, electron density at HOMO of inhibitor **(III)** and **(IV)** is more than those of inhibitor **(I)** and **(II)**. It is expected that corrosion inhibition efficiency of **(III)** and **(IV)** is better than those of inhibitor **(I)** and **(II)**. As for the contour diagram of LUMO, if studied compounds accept electron from metal, these electrons will be mainly delocalized on the structure. The other part to be examined is MEP maps and contours. They calculated at HF/6-31G(d) level in gas phase and represented in Fig. 3.

According to Fig. 3, the reactivity of heteroatoms is not as much as expected. Because there are not so many red or yellow regions in the environment of heteroatoms. Additionally, it is easily seen that the steric effects are dominant in the environment of heteroatoms. In determination of corrosion mechanism, molecular structure is so important. If optimized structures are examined in detail, molecular planarity in inhibitor **(III)** and **(IV)** is more than those of others. It is understood that surface area among related inhibitors and metal is more than those of others. Also, inhibition efficiencies of inhibitor **(III)** and **(IV)** are better than those of inhibitor **(I)** and **(II)**. The other important stage is the determination of corrosion mechanism is NBO analyses. The stabilization energy of the second order perturbation theory is mainly associated with delocalization. Lower stabilization energy is mean that better inhibition efficiency. The lowest stabilization energy is calculated as -506.27, -2057.92, -530.24 and -453.69 kcal mol^{-1} for inhibitor **(I)** – **(IV)**, respectively. According to these results, it is expected that inhibitor **(IV)** is the best corrosion inhibitor. The last one is Fukui functions for electrophilic, nucleophilic and radicalic attacks. Fukui functions are calculated at HF/6-31G(d) level in gas phase via using Eq. (10) – (12) and they are given in Table 3 for heteroatoms.

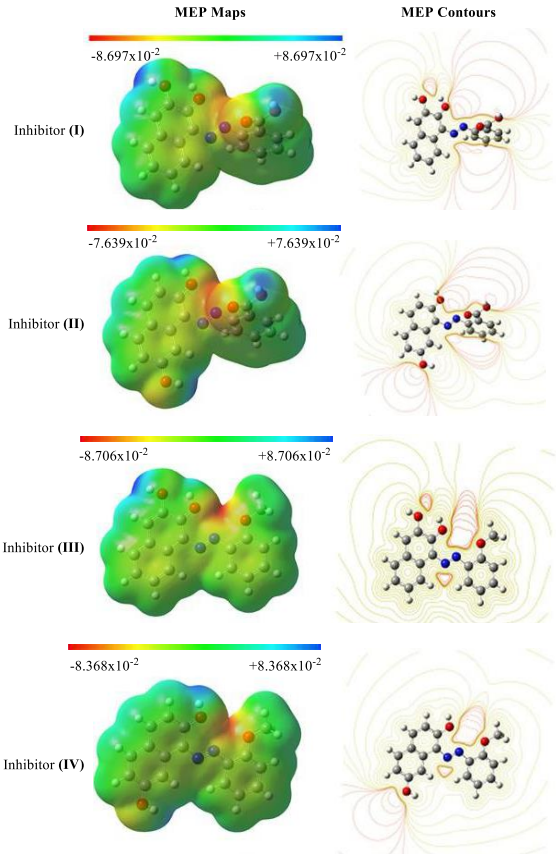

Fig. 3. MEP maps and contours of investigated chemicals at HF/6-31G(d) level in vacuum.

Table 3. Calculated condensed Fukui functions for heteroatom in mentioned molecules

Inhibitors	Atoms	$P_k(N+1)$	$P_k(N)$	$P_k(N-1)$	f_k^+	f_k^0	f_k^-
Inhibitor **(I)**	N1	7.434	7.191	7.105	0.24292	0.16463	0.08634
	N2	7.397	7.129	6.738	0.26769	0.329545	0.39140
	O1	8.735	8.737	8.748	-0.00218	-0.00693	-0.01167
	O2	8.789	8.771	8.765	0.01749	0.01178	0.00607
	O3	8.748	8.681	8.683	0.06744	0.03251	-0.00242
	O4	8.756	8.782	8.761	-0.02524	-0.00225	0.02074
Inhibitor **(II)**	N1	7.426	7.190	7.109	0.23628	0.15884	0.08140
	N2	7.407	7.143	6.744	0.26375	0.33169	0.39963
	O1	8.726	8.726	8.747	0.00018	-0.01036	-0.0209
	O2	8.769	8.745	8.734	0.02369	0.01757	0.01145
	O3	8.750	8.681	8.685	0.06873	0.03268	-0.00337
	O4	8.756	8.782	8.761	-0.02591	-0.00241	0.02109
Inhibitor **(III)**	N1	7.476	7.224	7.107	0.25161	0.18440	0.11719
	N2	7.348	7.134	6.755	0.21450	0.296435	0.37837
	O1	8.732	8.718	8.746	0.01448	-0.00699	-0.02847
	O2	8.787	8.773	8.765	0.01422	0.01092	0.00762
	O3	8.589	8.587	8.605	0.00184	-0.00783	-0.01750
Inhibitor **(IV)**	N1	7.466	7.218	7.108	0.24792	0.17882	0.10972
	N2	7.361	7.147	6.762	0.21373	0.29922	0.38471
	O1	8.723	8.710	8.745	0.01281	-0.01110	-0.03500
	O2	8.771	8.746	8.734	0.02504	0.01843	0.01182
	O3	8.590	8.588	8.606	0.00178	-0.00809	-0.01797

According to Table 3, N2 atom is appropriate for electrophilic, nucleophilic and radicalic attacks in inhibitor **(I)** and **(II)** while N1, N2 ve N2 atoms is appropriate for nucleophilic, radicalic and electrophilic attacks, respectively in inhibitor **(III)** and **(IV)**.

As a result, The N1 and N2 atoms are in the interior of the molecules and sterically crowded. Thence, it is thought that inhibitors will protect the metal horizontally rather than a single point. Also, due to their planarity, inhibition efficiencies of inhibitor **(III)** and **(IV)** are better than those of **(I)** and **(II)**. In terms of NBO analysis, inhibitor **(IV)** is the best molecule in protection of metal in corrosion. All these results are appropriate with experimental results. The inhibitors cover the surface of the metal horizontally.

3.4. Regression Analyses and Theoretical Formula

Regression analyses is important step in search of harmony between experimental and calculated results. The scatter graphs are plotted by using experimental inhibition efficiencies and quantum chemical parameters. These graphs are represented in Supp. Fig. S1 – S6 for each quantum chemical descriptors, respectively. According to these graphs, E_{HOMO}, E_{LUMO}, E_{GAP} and chemical softness are the most compatible descriptors. They are used to derived new theoretical formula for derivatives of mono azo naphthylamine dyes. This formula is given in Eq. (13).

$$\%IE_{Teorik} = 5504.34 \times E_{HOMO} + 5599.49 \times E_{LUMO} - 5530.34 \times E_{GAP} + 666.49 \times \sigma \quad (13)$$

Eq. (13) is obtained by regression analysis and matrix solution. Experimental inhibition efficiencies of inhibitor **(I)** – **(IV)** have been reported as 81.08, 83.76, 87.19 and 88.73, respectively while they calculated as 81.00, 83.68, 87.11 and 88.65, respectively. The scatter graph is plotted by using these values and represented in Fig. 4.

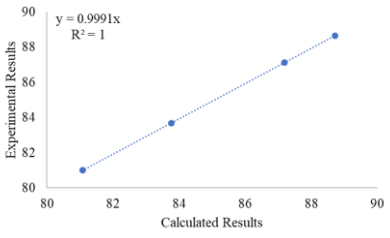

Fig. 4. The scatter graph between experimental and calculated inhibition efficiencies.

According to Fig. 4, correlation coefficient (R^2) indicates the orientation between the experimental and calculated results. The orientation is good for our studied molecules. The agreement between related results can be handled by graphic slope. Graphic slope of our graphic is calculated as 0.9991. It indicates that, there is a well agreement between experimental and calculated results.

4. Conclusion

Studied mono azo naphthylamine compounds are optimized at HF/6-31G(d), B3LYP/6-31G(d) and M062X/6-31G(d) levels in gas phase. Quantum chemical descriptors of mentioned molecules are calculated in each level and compared with experimental ones. The best method is determined as HF/6-31G(d) level and this level is taken into consideration in calculation of MEP maps, MEP contours, HOMO and LUMO contour diagram, NBO calculations, optimization in water and condensed Fukui functions. All quantum chemical parameters are compared with experimental inhibition efficiency and compatible descriptors are determined by regression analyses. Then, a new theoretical formula for aluminum is derived by matrix solution. The well agreement is calculated between experimental and calculated inhibition efficiencies.

Acknowledgment

This work is supported by the Scientific Research Project Fund of Cumhuriyet University under the project number F-490. This research is made possible by TUBITAK ULAKBIM, High Performance and Grid Computing Center (TR-Grid e-Infrastructure).

References

[1] Yuxi Zhao, Xiaowen Zhang, Weiliang Jin, Influence of environment on the development of corrosion product-filled paste and a corrosion layer at the steel/concrete interface, Corrosion Science http://dx.doi.org/10.1016/j.corsci.2017.03.026.

[2] D.-H. Xia, et al., Atmospheric corrosion assessed from corrosion images using fuzzy Kolmogorov–Sinai entropy, Corros. Sci. (2017), http://dx.doi.org/10.1016/j.corsci.2017.02.015.

[3] N.D. Alexopoulos, et al., Synergy of corrosion-induced micro-cracking and hydrogen embrittlement on the structural integrity of aluminium alloy (Al-Cu-Mg) 2024, Corros. Sci. (2017), http://dx.doi.org/10.1016/j.corsci.2017.03.001.

[4] Jinlong Wang, Minghui Chen, Yuxian Cheng, Lanlan Yang, Zebin Bao, Li Liu, Shenglong Zhu, Fuhui Wang, Hot corrosion of arc ion plating NiCrAlY and sputtered nanocrystalline coatings on a nickel-based single-crystal superalloy, Corrosion Sciencehttp://dx.doi.org/10.1016/j.corsci.2017.04.004.

[5] Yuxi Zhao, Xiaowen Zhang, Weiliang Jin, Influence of environment on the development of corrosion product-filled paste and a corrosion layer at the steel/concrete interface, Corrosion Sciencehttp://dx.doi.org/10.1016/j.corsci.2017.03.026.

[6] L. Wei, et al., Effect of exposure angle on the corrosion behavior of X70 steel under supercritical CO2 and gaseous CO2 environments, Corros. Sci. (2017), http://dx.doi.org/10.1016/j.corsci.2017.03.011.

[7] Y. Han, et al., Effects of electropolishing on corrosion and stress corrosion cracking of Alloy 182 in high temperature water, Corros. Sci. (2017), http://dx.doi.org/10.1016/j.corsci.2017.03.004.

[8] T.J. Watson, et al., Salt fog corrosion behavior in a powder-processed icosahedral-phase-strengthened aluminum alloy, Corros. Sci. (2017), http://dx.doi.org/10.1016/j.corsci.2017.03.010.

[9] H.N. Krogstad, R. Johnsen, Corrosion properties of nickel-aluminium bronze in natural seawater—Effect of galvanic coupling to UNS S31603, Corros. Sci. (2017), http://dx.doi.org/10.1016/j.corsci.2017.03.016.

[10] Xianghong Li, Shuduan Deng, Tong Lin, Xiaoguang Xie, Guanben Du, 2-Mercaptopyrimidine as an effective inhibitor for the corrosion of cold rolled steel in HNO3 solution, Corrosion Science 118 (2017) 202–216.

[11] Y. Qiang, et al., Experimental and theoretical studies of four allyl imidazolium-based ionic liquids as green inhibitors for copper corrosion in sulfuric acid, Corros. Sci. (2017), http://dx.doi.org/10.1016/j.corsci.2017.02.021.

[12] Zohreh Salarvand, Mehdi Amirnasr, Milad Talebian, Keyvan Raeissi, Soraia Meghdadi, Enhanced corrosion resistance of mild steel in 1 M HCl solution by trace amount of 2-phenyl-benzothiazole derivatives: Experimental, quantum chemical calculations and molecular dynamics (MD) simulation studies, Corrosion Science 114 (2017) 133–145.

[13] . M. Mabrouk, H. Shokry, K. M. Abu Al-Naja, Inhibition of aluminum corrosion in acid solution by mono- and bis-azo naphthylamine dyes. Part 1, Chem Met Alloys 4 (2011) 98–106.

[14] GaussView, Version 5, Roy Dennington, Todd Keith, and John Millam, Semichem Inc., Shawnee Mission, KS, 2009.

[15] Gaussian 09, Revision A.02, M. J. Frisch, G. W. Trucks, H. B. Schlegel, G. E. Scuseria, M. A. Robb, J. R. Cheeseman, G. Scalmani, V. Barone, B. Mennucci, G. A. Petersson, H. Nakatsuji, M. Caricato, X. Li, H. P. Hratchian, A. F. Izmaylov, J. Bloino, G. Zheng, J. L. Sonnenberg, M. Hada, M. Ehara, K. Toyota, R. Fukuda, J. Hasegawa, M. Ishida, T. Nakajima, Y. Honda, O. Kitao, H. Nakai, T. Vreven, J. A. Montgomery, Jr., J. E. Peralta, F. Ogliaro, M. Bearpark, J. J. Heyd, E. Brothers, K. N. Kudin, V. N. Staroverov, R. Kobayashi, J. Normand, K. Raghavachari, A. Rendell, J. C. Burant, S. S. Iyengar, J. Tomasi, M. Cossi, N. Rega, J. M. Millam, M. Klene, J. E. Knox, J. B. Cross, V. Bakken, C. Adamo, J. Jaramillo, R. Gomperts, R. E. Stratmann, O. Yazyev, A. J. Austin, R. Cammi, C. Pomelli, J. W. Ochterski, R. L. Martin, K. Morokuma, V. G. Zakrzewski, G. A. Voth, P. Salvador, J. J. Dannenberg, S. Dapprich, A. D. Daniels, Ö. Farkas, J. B. Foresman, J. V. Ortiz, J. Cioslowski, and D. J. Fox, Gaussian, Inc., Wallingford CT, 2009.

[16] Gaussian 09, Revision D.01, M. J. Frisch, G. W. Trucks, H. B. Schlegel, G. E. Scuseria, M. A. Robb, J. R. Cheeseman, G. Scalmani, V. Barone, B. Mennucci, G. A. Petersson, H. Nakatsuji, M. Caricato, X. Li, H. P. Hratchian, A. F. Izmaylov, J. Bloino, G. Zheng, J. L. Sonnenberg, M. Hada, M. Ehara, K. Toyota, R. Fukuda, J. Hasegawa, M. Ishida, T. Nakajima, Y. Honda, O. Kitao, H. Nakai, T. Vreven, J. A. Montgomery, Jr., J. E. Peralta, F. Ogliaro, M. Bearpark, J. J. Heyd, E. Brothers, K. N. Kudin, V. N. Staroverov, R. Kobayashi, J. Normand, K. Raghavachari, A. Rendell, J. C. Burant, S. S. Iyengar, J. Tomasi, M. Cossi, N. Rega, J. M. Millam, M. Klene, J. E. Knox, J. B. Cross, V. Bakken, C. Adamo, J. Jaramillo, R. Gomperts, R. E. Stratmann, O. Yazyev, A. J. Austin, R. Cammi, C. Pomelli, J. W. Ochterski, R. L. Martin, K. Morokuma, V. G. Zakrzewski, G. A. Voth, P. Salvador, J. J. Dannenberg, S. Dapprich, A. D. Daniels, Ö. Farkas, J. B. Foresman, J. V. Ortiz, J. Cioslowski, and D. J. Fox, Gaussian, Inc., Wallingford CT, 2009.

[17] PerkinElmer, 2012. ChemBioDraw Ultra Version (13.0.0.3015), CambridgeSoft Waltham, MA, USA.

[18] C. C. J. Roothaan, New Developments in Molecular Orbital Theory, Rev Mod Phys 23 (1951) 69.

[19] A. D. Becke, Density-functional thermochemistry. III. The role of exact exchange, J Chem Phys 98 (1993) 5648-5652.

[20] Y. Zhao, D. G. Truhlar, The M06 suite of density functionals for main group thermochemistry, thermochemical kinetics, noncovalent interactions, excited states, and transition elements: Two new functionals and systematic testing of four M06-class functionals and 12 other functionals". Theor Chem Account 120 (2006) 215–241.

[21] K. Sayin, S. E. Kariper, T. A. Sayin, D. Karakaş, Theoretical spectroscopic study of seven zinc (II) complex with macrocyclic Schiff-base ligand. Spectrochimica Acta Part A: Molecular and Biomolecular Spectroscopy 133 (2014) 348-356.

[22] S. G. Sagdinc, D. Erdas, I. Gunduz, A. E. Sahinturk, FT-IR and FT-Raman spectra, molecular structure and first-order molecular hyperpolarizabilities of a potential antihistaminic drug, cyproheptadine HCl. Spectrochimica Acta Part A: Molecular

and Biomolecular Spectroscopy 134 (2015) 350-360.

[23] A. A. Soayed, A. F. El-Husseiny, Potentiometry and geometrical structure of some azodye compounds and their metal complexes. Journal of Molecular Liquids 209 (2015) 258-266.

[24] W. H. Mahmoud, N. F. Mahmoud, G. G. Mohamed, A. A. El-Bindary, A. Z. El-Sonbati, Supramolecular structural, thermal properties and biological activity of 3-(2-methoxyphenoxy) propane-1, 2-diol metal complexes. Journal of Molecular Structure 1086 (2015) 266-275.

[25] A. Z. El-Sonbati, M. A. Diab, A. A. El-Bindary, M. M. Ghoneim, M. T. Mohesien, M. A. El-Kader, Polymeric complexes—LXI. Supramolecular structure, thermal properties, SS-DNA binding activity and antimicrobial activities of polymeric complexes of rhodanine hydrazone compounds. Journal of Molecular Liquids 215 (2016) 711-739.

[26] A. A. El-Bindary, M. M. Ghoneim, M. A. Diab, A. Z. El-Sonbati, L. S. Serag, Thermodynamic studies of N-allylrhodanine derivatives and their metal complexes. Journal of Molecular Liquids 223 (2016) 448-461.

[27] K. Sayin, N. Kurtoglu, M. Kose, D. Karakas, M. Kurtoglu, Computational and experimental studies of 2-[(E)-hydrazinylidenemethyl]-6-methoxy-4-[(E)-phenyldiazenyl] phenol and its tautomers. Journal of Molecular Structure 1119 (2016) 413-422.

[28] Ayhan Üngördü, Nurten Tezer, The solvent (water) and metal effects on HOMO-LUMO gaps of guanine base pair: A computational study, Journal of Molecular Graphics and Modellinghttp://dx.doi.org/10.1016/j.jmgm.2017.04.015.

[29] T Koopmans, Über die Zuordnung von Wellenfunktionen und Eigenwerten zu den Einzelnen Elektronen Eines Atoms, Physica 1 (1934) 104–113.

[30] Nihat Karakus, Koray Sayin, The investigation of corrosion inhibition efficiency on some benzaldehyde thiosemicarbazones and their thiole tautomers: Computational study, Journal of the Taiwan Institute of Chemical Engineers 48 (2015) 95–102.